Aging disrupts muscle stem cell function by impairing matricellular WISP1 secretion from fibro-adipogenic progenitors

Laura Lukjanenko, Sonia Karaz, Pascal Stuelsatz, Uxia Gurriaran-Rodriguez, Joris Michaud, Gabriele Dammone, Federico Sizzano, Omid Mashinchian, Sara Ancel, Eugenia Migliavacca, et al.

HHS Public Access

Author manuscript

Cell Stem Cell. Author manuscript; available in PMC 2020 March 07.

Published in final edited form as:

Cell Stem Cell. 2019 March 07; 24(3): 433–446.e7. doi:10.1016/j.stem.2018.12.014.

Aging Disrupts Muscle Stem Cell Function by Impairing Matricellular WISP1 Secretion from Fibro-Adipogenic Progenitors

Laura Lukjanenko[#1,2], **Sonia Karaz**[#1], **Pascal Stuelsatz**[1], **Uxia Gurriaran-Rodriguez**[3,4], **Joris Michaud**[1], **Gabriele Dammone**[1], **Federico Sizzano**[1], **Omid Mashinchian**[1,2], **Sara Ancel**[1,2], **Eugenia Migliavacca**[1], **Sophie Liot**[5], **Guillaume Jacot**[1], **Sylviane Metairon**[1], **Frederic Raymond**[1], **Patrick Descombes**[1], **Alessio Palini**[1], **Benedicte Chazaud**[5], **Michael A. Rudnicki**[3,4], **C. Florian Bentzinger**[1,6], and **Jerome N. Feige**[1,2]

[1.]Nestlé Research, EPFL Innovation Park, 1015 Lausanne, Switzerland [2.]School of Life Sciences, Ecole Polytechnique Federale de Lausanne (EPFL), 1015 Lausanne, Switzerland [3.]Sprott Center for Stem Cell Research, Ottawa Hospital Research Institute, Ottawa, ON K1H8L6, Canada [4.]Department of Cellular and Molecular Medicine, Faculty of Medicine, University of Ottawa, Ottawa, Canada [5.]Institut NeuroMyoGène, Université Claude Bernard Lyon 1, CNRS 5310, INSERM U1217, Lyon, France [6.]Département de pharmacologie et physiologie, Faculté de médecine et des sciences de la santé, Université de Sherbrooke, Qc, Canada

[#] These authors contributed equally to this work.

Summary

Research on age-related regenerative failure of skeletal muscle has extensively focused on the phenotypes of muscle stem cells (MuSCs). In contrast, the impact of aging on regulatory cells in the MuSC niche remains largely unexplored. Here, we demonstrate that aging impairs the function of mouse fibro-adipogenic progenitors (FAPs) and thereby indirectly affects the myogenic potential of MuSCs. Using transcriptomic profiling, we identify WNT1 Inducible Signaling Pathway Protein 1 (WISP1) as a FAP-derived matricellular signal that is lost during aging. WISP1 is required for efficient muscle regeneration and controls the expansion and asymmetric commitment of MuSCs through Akt signaling. Transplantation of young FAPs or systemic treatment with WISP1 restores the myogenic capacity of MuSCs in aged mice and rescues skeletal

Author contributions

L.L. and J.N.F initiated and managed the project. L.L., S.K., P.S., U.G.R., J.M., G.D., F.S., O. M., S.A., S.L., B.C. designed and conducted experiments, and analyzed data. E.M. and F.R. performed genomic data analysis. S.M., G.J., A.P and P.D supported imaging, flow cytometry or genomics. M.A.R. provided critical reagents and interpreted the results. L.L., P. S., C.F.B. and JNF interpreted the results and wrote the manuscript.

Lead contact: Jerome N. Feige, Jerome.Feige@rd.nestle.com

Competing financial interests

All authors except U.G.R, S.L., B.C. and M.A.R. are or were employees of the Nestle Institute of Health Sciences / Nestec S.A., Switzerland. L.L. and J.N.F. are inventors of patent WO2017207678A1 assigned to Nestec S.A.

muscle regeneration. Our work establishes that loss of WISP1 from FAPs contributes to MuSC dysfunction in aged skeletal muscles and demonstrate that this mechanism can be targeted to rejuvenate myogenesis.

Graphical Abstract

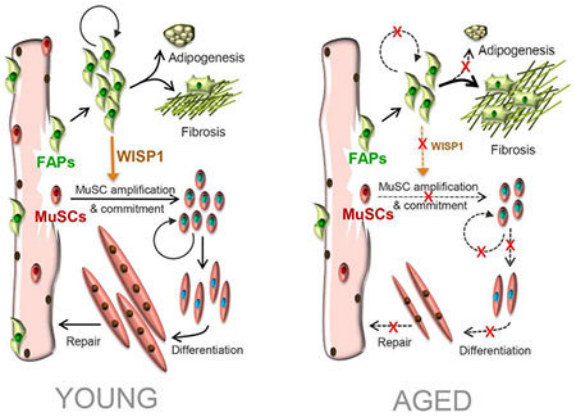

eTOC blurb:

Feige and colleagues report that aging impairs matricellular signals in the skeletal muscle stem cell niche by affecting the function of fibro-adipogenic progenitors (FAPs). Aged FAPs secrete less matricellular WISP1 leading to impaired myogenic commitment of muscle stem cells (MuSCs). Restoration of WISP1 levels in the aged niche rejuvenates MuSCs and improves muscle regeneration.

Keywords

Muscle Stem Cells; Matricellular Signaling; Skeletal Muscle; Aging; Stem Cell Niche; Fibro-Adipogenic Progenitors; WISP1

Introduction

The regenerative capacity of skeletal muscle depends on the activity of tissue-resident muscle stem cells (MuSCs), also termed satellite cells. As a consequence of aging, the regenerative function of MuSCs is dramatically impaired, leading to inefficient muscle repair following injury (Almada and Wagers, 2016; Blau et al., 2015; Brack and Munoz-Canoves, 2015). The number of MuSCs decreases in aged muscle (Shefer et al., 2006), and remaining cells display impaired activation, adhesion, migration, proliferation, self-renewal and differentiation, and gradually switch to a senescent phenotype (Lukjanenko et al., 2016; Price et al., 2014; Sousa-Victor et al., 2014; Tierney et al., 2018). Alterations in both cellular signaling pathways and metabolism have been shown to impair MuSC function during aging. Aged MuSCs exhibit increased p38-mitogen-activated protein kinase (MAPK), ERK/MAPK and JAK/STAT signaling (Bernet et al., 2014; Chakkalakal et al., 2012; Cosgrove et al., 2014; Price et al., 2014; Sousa-Victor et al., 2014), as well as Hoxa9 induction in response to epigenetic stress (Schworer et al., 2016). In addition, impaired mitochondrial

function as well as decreased autophagy perturb the physiology of MuSCs during aging and accelerate their transition towards senescence (Garcia-Prat et al., 2016; Zhang et al., 2016). Importantly, recent studies have begun to elucidate the nature of the extracellular signals which are disrupted in the niche and mediate some of these long-lasting intrinsic adaptations. For example, alterations in the levels of Fibronectin, Notch ligands, fibroblast growth factor (FGF)-2, Wnt ligand C1q, transforming growth factor (TGF-) β, oxytocin or apelin, have been reported to affect cellular aging pathways and thereby disturb MuSC function (Brack et al., 2007; Carlson et al., 2008; Chakkalakal et al., 2012; Elabd et al., 2014; Lukjanenko et al., 2016; Naito et al., 2012; Price et al., 2014; Vinel et al., 2018; Wang et al., 2015). Yet, in-spite of these fundamental advancements in our understanding of the muscle stem cell niche, the cellular origin of extrinsic MuSC regulatory signals that are affected by the aging process remain largely enigmatic.

During adult myogenesis, MuSC function is under the control of a wide range of paracrine signals originating from different cell types in the niche (Mashinchian et al., 2018). The regulatory interplay between MuSCs, immune cells, fibrogenic cells and adipogenic progenitors has emerged to be of particular complexity (Heredia et al., 2013; Varga et al., 2016; Verma et al., 2018). Reciprocal control of MuSCs and fibroblasts is indispensable for efficient expansion of the MuSC pool and for keeping interstitial fibrosis in check (Fry et al., 2016; Murphy et al., 2011). Similarly, ablation of lineages with adipogenic potential leads to dysfunctional muscle repair (Liu et al., 2012). Both fibroblast-like cells and adipocytes residing in skeletal muscle are derived from a common bipotent mesenchymal fibro/adipogenic progenitor (FAP) marked by the expression of the platelet-derived growth factor receptor (PDGFR) α (Joe et al., 2010; Liu et al., 2012; Uezumi et al., 2010). Upon muscle injury, FAPs activate, enter a proliferative phase at the same time as MuSCs and support myogenic commitment (Joe et al., 2010). Altered FAP lineage decisions during regeneration perturb ECM remodeling and impair myogenesis (Fiore et al., 2016; Mozzetta et al., 2013). Permissive changes in the micro-environment of diseased muscle and altered FAP apoptosis in the late phase of regeneration promotes excessive differentiation towards fat or fibrotic tissue (Heredia et al., 2013; Lemos et al., 2015; Uezumi et al., 2010). One of the signals involved in fibrotic fate decisions of FAPs is platelet-derived growth factor (PDGF), which can be dynamically regulated by alternative processing of the *Pdgfra* mRNA in FAPs during muscle regeneration (Mueller et al., 2016). These observations demonstrate that FAPs orchestrate a plethora of processes involved in regenerative myogenesis and highlight the need for a better understanding of the signals controlling MuSC function.

Notably, aging affects mesenchymal progenitors in multiple tissues (Raggi and Berardi, 2012). Similarly, oxidative stress and other senescence-associated processes impair adipogenic progenitors in aged fat tissue (Tchkonia et al., 2010). These observations suggest that FAPs and their support function for myogenesis could also be deregulated by the aging process. Here, we set out to test this hypothesis and demonstrate that FAP activity is severely impaired as a consequence of old age. We describe that aged FAPs fail to support MuSCs due to reduced secretion of the matricellular protein WNT1 Inducible Signaling Pathway Protein 1 (WISP1). FAP-secreted WISP1 controls asymmetric MuSC commitment and activates the Akt pathway. Similar to aging, genetic deletion of WISP1 in mice perturbs the MuSC pool and impairs myogenesis. Conversely, systemic treatment of aged mice with

recombinant WISP1, or transplantation of young but not aged or WISP1 knock-out FAPs, rescues MuSC function and rejuvenates the regenerative capacity of aged skeletal muscle. In summary, we demonstrate that the regenerative failure inherent to aged muscle can be ameliorated by targeting matricellular communication between FAPs and MuSCs.

Results

Aging affects FAP function

Given the negative impact of aging on mesenchymal stem cells (Raggi and Berardi, 2012) and the pivotal role of FAPs as support cells in the MuSC niche (Joe et al., 2010; Lemos et al., 2015; Uezumi et al., 2010), we first asked whether FAP function is affected during aging. To address this question, we collected FAPs and MuSCs from muscles of 9-13 week-old young mice and 20-25 month-old pre-geriatric aged mice (Sousa-Victor et al., 2014) using fluorescence-activated cell sorting (FACS; Figure S1A). Ex-vivo culture of MuSCs confirmed previously described aging defects that included impaired proliferation, reduced upregulation of the myogenic commitment factor MyoD and inefficient differentiation of aged MuSCs (Figures S1B-S1E). Notably, we observed that aged FAPs also displayed a range of altered cellular phenotypes. In ex-vivo culture, the number of FAPs isolated from aged mice was reduced and they incorporated less EdU compared to young controls (Figures 1A-1C). Immunostaining for PDGFRα revealed lower numbers of FAPs in muscles of aged mice (Figure S1F and S1G). To investigate how aging affects FAP levels during regeneration, we analyzed muscles at different time-points after injury. This revealed decreased numbers of aged FAPs at 4 days post injury (dpi), that failed to be cleared from the tissue at 7 dpi (Fig. S1H and S1I). Functional ex-vivo analysis of aged FAPs demonstrated impaired growth factor induced (Figures 1D and 1E) and spontaneous (Figure S2A) adipogenesis. Clonal analysis of single aged FAPs showed that the capacity for expansion and the number of adipogenic clones are reduced compared to the young condition (Figure S2B). No difference in differentiation was observed between young and aged FAPs once the cells have taken a fate decision and an adipogenic clone had emerged (Figure S2C), indicating that aging affects fate decisions at the progenitor level. The impaired adipogenic potential of aged FAPs was reflected by reduced levels of Oil red O positive intramuscular adipocytes at 14 dpi (Figures 1F, 1G **and** S2D). This effect was also observed in hematoxylin/eosin stainings (Figure S2E) and confirmed by the quantification of perilipin-positive adipocytes in cross-sections of aged muscles at 14 dpi (Figures S2F and S2G). In contrast, fibrogenic FAP differentiation to α-smooth muscle actin and collagenIα1 positive cells was higher in aged FAPs (Figures 1H, 1I **and** S2H). In agreement with these findings, masson trichrome staining of muscle cross-sections of young and aged mice showed elevated fibrosis in aged muscle both before and after injury (Figures 1J and 1K). Gene expression profiling of young and aged FAPs isolated from injured muscles at 7dpi further confirmed this finding and revealed increased mRNA expression of the GO term “Extracellular matrix” (Figures S2I and S2J). Fibrotic and adipogenic fate decisions in FAPs have been recently demonstrated to be mediated by alternative processing of the PDGFRα transcript (Mueller et al., 2016). An intronic variant of PDGFRα coding for a protein isoform with a truncated kinase domain acts as a decoy receptor to inhibit PDGF signaling and inhibit FAP differentiation into fibrotic cells. Interestingly, we observed that the relative

amounts of this PDGFRα intronic variant (PDGFRα-In) is reduced after injury in aged muscles as well as in aged FAPs following FACS isolation (Figures 1L and 1M). Collectively, these data demonstrate that the function of aged FAPs is perturbed and that aging uncouples adipogenic from fibrogenic fate decisions at the progenitor level.

Aged FAPs fail to support MuSCs.

Following injury, FAPs initially expand to support MuSC function (Fiore et al., 2016; Joe et al., 2010; Mozzetta et al., 2013). In order to characterize the cellular cross-talk between FAPs and MuSCs in a system where the age of each cell type can be uncoupled, we isolated MuSCs from tdTomato (Td) mice (Prigge et al., 2013), which constitutively express a nuclear red fluorescent protein (Figure S3A). The cells were then tracked based on the reporter in co-cultures with wild-type (WT) FAPs (Figures 2A **and** S3B). Aged FAPs displayed a reduced ability to support MuSC expansion and differentiation (Figures 2B-2D). The positive effect of FAPs on MuSC expansion correlated with the amount of FAPs (Figure S3C) and was not due to effects on the viability of MuSCs (Figure S3D). We next tested whether FAPs support MuSCs through soluble factors. Using single myofiber cultures, we demonstrated that the proliferation of MuSCs was increased in the presence of medium conditioned by young FAPs, but was unaffected by medium conditioned by aged FAPs (Figures 2E and 2F). FAP conditioned culture medium was also able to promote the proliferation and differentiation of MuSCs ex-vivo (Figures S3E and S3F). Thus, aging impairs the secretion of a soluble myogenic support signal from FAPs.

WISP1 is secreted by activated FAPs and is lost during aging

To uncover the molecular nature of the FAP-derived MuSC support signal lost during aging, we profiled the transcriptome of FAPs and MuSCs that were isolated in injured and uninjured muscles from young and aged mice. We first analyzed the gene ontology (GO) terms enriched in FAPs compared to MuSCs, and identified strong signatures of “organ development”, “cell adhesion”, and “extracellular matrix organization” in FAPs (Table S1). The fibrogenic nature of FAPs was highlighted by the higher expression of genes of the “extracellular matrix” GO term (Figure S4), and aging enhanced both molecular regulators of fibrosis in quiescent FAPs (Table S2) and ECM/fibrosis signatures at 7dpi (Figures S2I and S2J). We next examined which transcripts coding for secreted proteins were upregulated in activated FAPs. Out of the 321 genes significantly upregulated with a fold-change >2 during activation of young FAPs, we identified 20 secreted signaling proteins (Figure 3A). Genes upregulated in activated FAPs were then filtered for differential regulation with age and activation. The resulting 10 transcripts differentially regulated in aged activated FAPs contained a single secreted protein belonging to the CCN family of matricellular proteins and termed Wnt1 inducible signaling pathway protein 1 (WISP1 / CCN4) (Figure 3B). WISP1 was also the most down-regulated gene when aged activated FAPs were directly compared to young activated FAPs (Table S3). qPCR analysis confirmed that WISP1 is upregulated in young FAPs following muscle injury, and that this induction is blunted more than two-fold in FAPs from aged mice (Figure 3C). In agreement with these observations, the upregulation of WISP1 mRNA and protein was blunted in regenerating tibialis anterior muscles of aged mice (Figures 3D and 3E).

To confirm that FAPs are the principal cell type in which aging affects WISP1 secretion, we interrogated different cell types found in quiescent and regenerating muscles. These included lineage positive cells (Lin^+), comprising immune, endothelial and hematopoietic cells; MuSCs; FAPs; and $Sca1^+/CD34^+/PDGFR\alpha^-$ cells (hereafter called $PDGFR\alpha^-$). FAPs, MuSCs, and PDGFRα- cells upregulated WISP1 expression following injury, while very low expression was observed in Lin+ cells (Figure S5A). Notably, FAPs were the only cell type that displayed an age dependent reduction in WISP1 expression. Since WISP1 is a secreted protein, RNA FISH was used to elucidate where WISP1 is produced in skeletal muscle. Consistent with the localization of FAPs, we observed an upregulation of WISP1 mRNA granules typical of RNA FISH experiments in the interstitial space of regenerating muscles (Figures S5B and S5C). No staining was detected in muscles of WISP1 knockout (WISP1−/−) mice. We also observed that WISP1 mRNA was not directly associated with MuSCs but frequently localized to the vicinity of these cells (Figure S5D). These results identify WISP1 as a FAP-derived MuSC support signal that is impaired during aging.

Loss of WISP1 impairs MuSC function and muscle regeneration

We next asked whether the loss of WISP1 is sufficient to impair muscle regeneration independently of other age-induced perturbations by analyzing WISP1−/− mice (Maeda et al., 2015). As expected, WISP1 mRNA was not detected in uninjured and regenerating WISP1−/− muscle (Figure S6A). We first assessed how loss of WISP1 affects the ex-vivo phenotype of MuSCs and FAPs. While WISP1−/− MuSCs did not display an altered proliferation or differentiation potential (Figures S6B-S6D), FAPs isolated from WISP1−/− mice increased in number (Figure S6E). Despite this phenotype, WISP1−/− FAPs were not able to support MuSCs as efficiently as WT FAPs (Figure 4A). Following in-vivo muscle injury, WISP1−/− muscles displayed reduced expression levels of myogenic markers such as Pax7, MyoD and Myogenin (Figures 4B-4D). Histologically, we observed a prominent reduction in committed Pax7+/MyoD+ MuSCs in muscle cross sections of WISP1−/− mice at 3 dpi (Figures 4E and 4F). At later stages of regeneration, the architecture of WISP1−/− muscles was perturbed and showed abnormally small myofibers (Figures 4G and 4H). In contrast, myofiber size was not affected by loss of WISP1 in uninjured muscle (Figure S6F), demonstrating that WISP1 impairs myofiber repair without promoting atrophy of healthy fibers. In addition, WISP1−/− mice displayed similar expression profiles of macrophage, immune, endothelial and fibroblast markers during regeneration (Figures S6G-S6J), suggesting that loss of WISP1 primarily affects the communication between FAPs and MuSCs. Altogether, these experiments demonstrate that loss of WISP1 from FAPs impairs MuSC function and recapitulates major age-associated phenotypes during skeletal muscle regeneration.

WISP1 increases MuSC commitment and activates the Akt pathway

Despite its matricellular nature, WISP1 is a soluble protein and can be detected in the systemic circulation (Maiese, 2014; Murahovschi et al., 2015). Addition of recombinant WISP1 to the culture medium increased the expansion and EdU incorporation of young and aged MuSCs ex-vivo (Figures 5A-5C, S7A and S7B), and promoted MuSC differentiation (Figure S7C). In contrast, WISP1 treatment did not affect FAP proliferation or myotube hypertrophy (Figures S7D and S7E). In order to interrogate effects on MuSC commitment,

WISP1 was added to the medium of cultured single myofibers isolated from Myf5-Cre-ROSA26-YFP reporter mice (Kuang et al., 2007). In this paradigm, WISP1 promoted the generation of committed Pax7+/Myf5+ MuSCs by stimulating the asymmetric division of Pax7+/Myf5-cells (Figures 5D and 5E). The Akt pathway has been implicated in asymmetric self-renewal defects of aged MuSCs (Rozo et al., 2016). Interestingly, WISP1 treatment of cultured myoblasts induced the phosphorylation of Akt (Figures 5F, 5G **and** S7F). Supporting the notion that WISP1 exerts its effects through the Akt pathway, treatment of freshly isolated MuSCs with an Akt inhibitor abrogated the beneficial effects of WISP1 on MuSC proliferation (Figure 5H). In conclusion, by stimulating pathways involved in proliferation and myogenic commitment, WISP1 positively influences processes altered during MuSC aging.

Transplantation of young FAPs rejuvenates aged MuSCs through WISP1

In order to demonstrate that WISP1 derived from FAPs stimulates MuSC function directly, we transplanted freshly isolated young, aged or WISP1−/− FAPs into regenerating muscles of WISP1−/− mice (Figure 6A). Young FAPs increased the number of Pax7+/MyoD+ MuSCs, while aged or WISP1−/− cells lost this effect (Figures 6B and 6C). Moreover, transplantation of young FAPs, but not aged or WISP1−/− FAPs, rescued the abundance of Pax7+/MyoD+ MuSCs in aged mice (Figure 6D and 6E). In conclusion, these experiments demonstrate that FAP-derived WISP1 directly stimulates the myogenic commitment of aged MuSCs through paracrine communication.

Systemic WISP1 treatment rescues MuSC function and regeneration in aged mice

We next set out to test whether a restoration of WISP1 levels can ameliorate the impaired regeneration of aged muscles. To this end, mice were treated by systemic injections of either recombinant WISP1 or vehicle during muscle regeneration. mRNA levels of Pax7, MyoD and Myogenin were significantly higher in WISP1-treated aged mice than in vehicle-treated animals at the myogenic peak of regeneration at 7dpi (Figures 7A-7C). In 3 dpi muscle cross sections of aged mice treated with WISP1, the number of MuSCs positive for the proliferation marker Ki67 was significantly increased when compared to the vehicle control (Figures 7D and 7E). WISP1 also restored the number of committed MyoD+ MuSCs in aged muscle (Figure 7F). Systemic treatment of aged mice with recombinant WISP1 did not alter the induction of macrophage, immune, endothelial and fibroblast markers during regeneration (Figures S7G-S7K). At later time-points of muscle regeneration, systemic WISP1 treatment restored the amount of newly formed embryonic myosin heavy chain positive (eMHC) fibers to the levels observed in the young controls (Figures 7G and 7H). WISP1 treatment also improved the overall architecture of aged regenerating muscles (Figure 7I) and resulted in significantly larger regenerating fibers indicative of more efficient regeneration and terminal myogenesis (Figure 7J). However, systemic WISP1 did not promote muscle growth and anabolism in non-injured muscle as myofiber size was not affected in contra-lateral muscles of aged WISP1-treated mice (Figure S7L). Thus, systemic WISP1 treatment rejuvenates the myogenic function of aged MuSCs and boosts muscle repair.

Discussion

In both mice and humans, aging leads to MuSC dysfunction and reduces the regenerative capacity of skeletal muscle (Almada and Wagers, 2016; Blau et al., 2015; Brack and Munoz-Canoves, 2015). Extensive efforts have aimed at understanding the mechanisms driving MuSC aging, which involve cell-autonomous processes and changes in the MuSC microenvironment (Bernet et al., 2014; Chakkalakal et al., 2012; Cosgrove et al., 2014; Garcia-Prat et al., 2016; Mashinchian et al., 2018; Price et al., 2014; Sousa-Victor et al., 2014; Zhang et al., 2016). The MuSC niche is highly complex and contains a flux of different cell types in a tightly controlled spatiotemporal manner. The regulation of MuSCs by local secretion of growth factors, extracellular matrix (ECM) and the presentation of cell-cell receptors in the niche depends on the function and proliferation kinetics of these niche cell populations. Since aging has been shown to affect several critical niche components, it is likely that the local deposition of these cues by niche-resident cells is particularly susceptible to age-induced stress. The identification of cell populations that fail to support MuSC function in aged muscles would allow for the development of targeted strategies to restore a youthful niche environment.

Here, we describe that aging severely perturbs the function of FAPs and their ability to support myogenesis. FAPs are less abundant and have an impaired proliferative capacity in aged muscle, but accumulate during the late stages of regeneration when they are normally cleared by apoptosis (Lemos et al., 2015). Using transcriptomic profiling we identified the matricellular protein WISP1 as a FAP-derived factor controlling MuSC expansion and commitment to myogenic differentiation. Age-induced loss of WISP1 is specific to the FAP population and directly deregulates MuSC function via paracrine signaling. Concomitantly, WISP1−/− mice phenocopy age-related defects of MuSC expansion, commitment, and muscle repair. WISP1 is part of the CCN family of matricellular proteins, and has previously been involved in ECM remodeling and tissue repair in bone, cartilage, gut and lung epithelium, skin, and the cardio-vascular system (Konigshoff et al., 2009; Maeda et al., 2015; Maiese, 2014; Ono et al., 2018; Quiros et al., 2017; Wright et al., 2018; Yoshioka et al., 2016). At the cellular level, WISP1 modulates survival and proliferation in a spectrum of biological settings (Maiese, 2014; Ono et al., 2018). CCN proteins possess four conserved functional domains through which they interact with the ECM, growth factors and cytokines (Maiese, 2014). Apart from their direct effects on cells, CCN proteins modulate the signaling efficiency of several growth factors (Maiese, 2014). These include VEGF and FGF (Lafont et al., 2005; Nishida et al., 2009), that have been shown to regulate MuSC function and muscle regeneration (Chakkalakal et al., 2012; Messina et al., 2007). Interestingly, WISP1 can interact with integrins via their cysteine-rich domains (Maiese, 2014; Ono et al., 2018). Integrin β1 activity is required for normal MuSC function, and is deregulated during aging (Rozo et al., 2016). Moreover, CCN proteins can bind to the niche ECM component Fibronectin that is critical for adhesion, survival and self-renewal of MuSCs and that is lost during regenerative remodeling of the aged stem cell niche (Bentzinger et al., 2013; Lukjanenko et al., 2016). Collectively, these observations suggest that FAP-derived matricellular WISP1 controls MuSC function in concert with growth factor signaling and the niche ECM.

Muscle regeneration associates with a transient ectopic adipocyte accumulation (Joe et al., 2010; Lukjanenko et al., 2013; Uezumi et al., 2010). Falling in line with the general paradigm that intra-muscular adipose tissue increases with advancing age and metabolic stress (Addison et al., 2014), fat infiltration following injury of aged muscle has also been proposed to become more abundant (Ikemoto-Uezumi et al., 2015). However, our data show that young mice with more efficient muscle repair activate stronger ectopic adipogenesis than aged mice. This observation is consistent with the reduced function of FAPs we observed in aged muscles. In line with our observation, aged mesenchymal progenitors from human white adipose tissue lose adipogenic potential (Tchkonia et al., 2010), and aged adipogenic progenitor senescence can be targeted to restore adipogenesis and metabolic homeostasis in adipose tissue (Xu et al., 2015). Interestingly, hind limb unloading after muscle injury impairs muscle regeneration, reduces ectopic adipogenesis and lowers expression of PDGFRα (Pagano et al., 2015), suggesting that, similar to aging, a deregulation of FAPs can alter muscle plasticity during immobility. Next to adipogenic conversion, the degree of fibrogenic FAP differentiation has also been shown to be of critical importance for normal muscle regeneration (Fiore et al., 2016). We observed that aging increases the fibrogenic signature of FAPs and primes them for fibrosis by reducing expression of the PDGFRα-In anti-fibrotic isoform that acts as a decoy receptor for PDGF (Mueller et al., 2016). Several inflammatory processes have been implicated in fibrosis in skeletal muscle (Mann et al., 2011). Interestingly, the inability of aged FAPs to efficiently attract regulatory T cells through the secretion of IL-33 has recently been described during muscle regeneration (Kuswanto et al., 2016). An important question arising from these observations is whether aging also affects the function of differentiated descendants of FAPs. Our clonal analysis revealed that aged FAPs have a reduced capacity for clonal expansion and fate decisions. However, following lineage commitment, the differentiation efficiency of clones derived from young and aged FAPs was similar. This implies that aging perturbs FAP function at the progenitor level, and thereby leads to a deregulation of MuSC function and a concomitant imbalance of adipogenic and fibrogenic fate decisions that further exacerbates the regenerative dysfunction of aged muscles.

During normal muscle regeneration, MuSCs undergo asymmetric divisions producing cells that upregulate myogenic regulatory factors and become committed to terminal differentiation (Kuang et al., 2007). Lower Fibronectin levels in the aged MuSC niche lead to a loss of Integrin β1 activation and are accompanied by a reduced sensitivity of the integrin associated FGF receptor (Bernet et al., 2014; Cosgrove et al., 2014; Rozo et al., 2016). These changes at the receptor level lead to a dysregulation of Akt, ERK and p38αβ MAPK pathways that impair the ability of aged MuSCs to undergo asymmetric commitment. Our experiments revealed that FAP-derived WISP1 activates the Akt pathway and has the ability to rescue age-associated commitment defects of MuSCs via asymmetric division. WISP1 can act through both paracrine production and systemic inter-organ communication (Maiese, 2014). Local paracrine secretion of WISP1 from young FAPs exogenously transplanted in aged muscle rescues commitment defects in aged MuSC, but loss of WISP1 expression in aged or WISP1−/− FAPs impairs this crosstalk. Moreover, systemic delivery of recombinant WISP1 in aged mice is able to restore MuSC function and muscle regeneration. Importantly, neither loss of WISP1 in knockout mice, nor WISP1

treatment affected the size of fibers in muscles that were not regenerating. These data demonstrate that the function of FAP-derived WISP1 in skeletal muscle is specific to regenerative myogenesis. In humans and mice, WISP1 contains 367 amino acids and has a comparably low molecular weight of ~40 kDa. In light of our study demonstrating systemic efficacy of WISP1 on MuSC function and regeneration, these favorable properties discern WISP1 as an attractive target for the future development of biologics that promote skeletal muscle repair.

Altogether, we discovered a major age-induced defect in the FAP compartment of skeletal muscle. We characterize WISP1 as a FAP-secreted molecule involved in the regulation of MuSCs that is lost from the aged niche and that can be supplied systemically to improve muscle healing in the aged.

STAR METHODS

CONTACT FOR REAGENT AND RESOURCE SHARING

Further information and requests for resources and reagents should be directed to and will be fulfilled by Dr Jerome N Feige (jerome.feige@rd.nestle.com).

EXPERIMENTAL MODELS

Mice were housed under standard conditions and allowed access to food and water ad libitum. All wildtype (WT) mice were C57BL/6JRj males purchased at the relevant age from Janvier labs. Young male mice were between 9-13 weeks old and aged male mice were 20-25 months. Heterozygous ROSA-nTnG (B6;129S6-Gt(ROSA)26Sortm4(CAG-tdTomato*,-EGFP*)Ees/J), hereafter called Td-Tomato mice were purchased from Jackson Labs and crossed onto a pure C57BL/6J genetic background to obtain homozygous mice used for isolation of MuSCs bearing a nuclear TdTomato fluorescent marker (Prigge et al., 2013). Heterozygous WISP1 (+/−) mice (B6; 129S6/SvEv-(WISP1-PKG-Neo)) were provided by Dr Marian Young (Maeda et al., 2015) and rederived through sperm insemination into C57/Bl6N mice. Heterozygous mice (95% pure) were then crossed together to obtain WISP1−/− mice and their WISP1+/+ littermate controls. Male adult Myf5-Cre/ROSA26-YFP mice (8 weeks of age) were obtained by crossing the knock-in Myf5-Cre (Tallquist et al., 2000) heterozygous mice with ROSA26-YFP homozygous reporter mice. Experiments with these latter mice were performed at the University of Ottawa, and all experimental procedures were approved by the University of Ottawa according to guidelines of the Canadian Council for Animal Care (CCAC). All other in vivo experiments were performed following the regulations of the Swiss Animal Experimentation Ordinance and approved by the ethical committee of the canton de Vaud under licenses VD2620, VD3002 and VD3199.

METHOD DETAILS

In vivo procedures (muscle regeneration, FAP transplantation & WISP1 treatment).—Muscle regeneration was induced by intramuscular injection of 50μl of 50% v/v glycerol into tibialis anterior (TA) muscles (experiments with WT mice) or 50μl of cardiotoxin 10μM (experiments with WISP1−/− mice, in vivo FAP quantification or FAP

transplantation), and mice were sacrificed 3, 4, 7 or 14 days post-injury (dpi). For isolation of muscle activated progenitors used for transcriptomics, tibialis anterior, quadriceps and gastrocnemius muscles were intramuscularly injected to maximize the number of cells collected, with 50μl, 50μl and 100μl of 50% v/v glycerol, respectively. For in vivo WISP1 treatment, mouse recombinant WISP1 protein (R&D # 1680-WS) was administered daily by intra-peritoneal injections at 1mg/kg per day during the course of muscle regeneration after injury. Young and aged control mice received an equivalent volume of PBS using the same dosing scheme. For in vivo FAP transplantation, FAPs were freshly isolated from uninjured muscles by flow cytometry and directly transplanted into regenerating tibialis anterior muscles by intra-muscular injection. 60'000 FAPs per mouse were co-injected with 0.02% w/v of fluorescent beads using a 50μl Hamilton syringe 24h after intra-muscular injection of 50μl of cardiotoxin 10μM.

Flow cytometry and progenitor cell isolation.—For isolation of cell populations, tibialis anterior, quadriceps and gastrocnemius muscles were collected uninjured or 3 days after glycerol injection and digested with Dispase II (2.5 U/ml) (Roche), Collagenase B (0.2%) (Roche) and MgCl2 (5 mM) at 37 °C. Cells were then incubated at 4 °C for 30 min with antibodies against CD45 (Invitrogen, MCD4501 or MCD4528; dilution for both 1/25), CD31 (Invitrogen, RM5201 or RM5228; dilution for both 1/25), CD11b (Invitrogen, RM2801 or RM2828; dilution for both 1/25), CD34 (BD Biosciences, 560230 or 560238; dilution for both 1/60), Ly-6A–Ly-6E (Sca1) (BD Biosciences, 561021; dilution 1/150), α7-integrin (R&D, FAB3518N; dilution 1/30) and CD140a (eBioscience, 12–1401–81 or 17–1401–81; dilution for both 1/30). Antibody validation is provided on the manufacturer's website. Specific cell subsets were isolated with a Beckman Coulter Astrios Cell sorter as described below and represented in supplementary figures S1 and S3A. MuSCs were identified as $CD31^{-}/CD11b^{-}/CD45^{-}/Sca1^{-}/CD34^{+}/Integrin\ \alpha7^{+}$ and Fibro/Adipogenic progenitors (FAPs) were identified as $CD31^{-}/CD11b^{-}/CD45^{-}/Sca1^{+}/CD34^{+}/PDGFR\alpha^{+}$. Lineage positive cells (Lin+) were identified as: $CD31^{+}/CD11b^{+}/CD45^{+}$. $CD31^{-}/CD11b^{-}/CD45^{-}/Sca1^{+}/CD34^{+}/PDGFR\alpha^{-}$ cells were also collected and named $PDGFR\alpha^{-}$ cells.

Single fiber isolation and effect of FAP-conditioned medium on single fibers.—Single myofibers were isolated and cultured ex vivo from the EDL muscles as previously described (Brun et al., 2018). Briefly, EDL muscles were harvested intact from tendon to tendon and enzymatically digested for 1h at 37C° with collagenase I (Worthington). Afterwards, single myofibers were manually separated and cultured in suspension in FAP-conditioned medium in 12-well plates, previously coated with horse serum to prevent fiber attachment. FAP-conditioned medium was prepared from young and aged FAPs isolated as described above, and cultured in fresh myofiber medium (15% FBS and 1% chick embryo extract (Accurate Chemicals)) in DMEM containing 2% L-glutamine, 4,5% glucose, and 110mg/ml sodium pyruvate at a density of 85000 FAPs/ml, for 24h before the medium was harvested to be used for single myofiber cultures. After 42h in culture, myofibers were then fixed with PFA 2%/PBS 1× for 10min at room temperature and then washed 3 times in PBS for 5min. Later myofibers were permeabilized for 10min with 0.1% Triton X-100, 0.1M Glycine in PBS 1× and followed by blocking solution for 2h at room temperature with 5% horse serum, 2% BSA, 0.1% Triton X-100 in PBS 1×. Incubation with undiluted Pax7

primary antibody (DHSB) was performed overnight. The following day, myofibers were washed 3 times in PBS for 5min and incubated with anti-mouse IgG1 in PBS for 1h at room temperature. Finally, myofibers were mounted with Mowiol medium containing Hoechst (10uL of Hoechst 1ug/uL). Total counting of Pax7+ and DAPI+ nuclei per myofiber was performed manually using an epifluorescent microscope Zeiss AxioObserver Z1. Digital images were taking using the same microscope.

Ex vivo assays.—MuSCs and FAPs were isolated by flow cytometry as described above, and unless otherwise mentioned, were directly plated into gelatin-coated 96 well plates and grown in 20mM glucose DMEM, 20% heat-inactivated FBS, 10% inactivated horse serum, 2.5ng/ml bFGF (Invitrogen), 1% P/S + 1% L+-Glutamine, 1% Na-pyruvate (Invitrogen), referred later as “growth medium”. MuSC viability was assessed at 12h post isolation using the HCS LIVE/DEAD Green Kit (Life Technologies). To asses MuSC cell cycle entry, 1μM EdU was added to the medium directly after cell sorting for 36h. To assess MuSC and FAP proliferation, 1μM EdU was added in the medium the third day after sorting for 3h, and the sixth day after sorting for 5h, respectively. MuSC differentiation was induced after four days of growth, by switching to differentiation medium (20mM glucose DMEM, 5% inactivated horse serum, 1% P/S) for 2 days. To test for adipogenic potential, FAPs were plated into Matrigel-coated 96 well plates and were either let to spontaneously differentiate for 13 days in growth medium, or switched to adipogenic differentiation medium on the sixth day for another seven days (20mM glucose DMEM, 20% heat-inactivated FBS, 1% P/S, 0,25μM dexamethasone, 1μg/ml insulin, 5μM troglitazone, 0.5mM isobutylmethylxanthine). To assess fibrogenic capacity, FAPs were grown for 6 days (α-SMA) or 10 days (Col1a1) in growth medium. For co-cultures, unless stated otherwise, the same number of MuSCs and FAPs/MuSCs were seeded in wells. When conditioned medium was used, all cells were freshly isolated the same day, and transfer of conditioned medium to MuSCs was performed after 1 day, then daily during the entire protocol. For WISP1 ex vivo treatment experiments, 8μg/mL of mouse recombinant WISP1 protein (R&D # 1680-WS) or human recombinant WISP1 protein (Peprotech, # 120-18), or equal amount of vehicle was added in the medium. Medium containing WISP1 or vehicle was changed daily. To avoid batch to batch variation in the efficacy of recombinant WISP1, all new commercial batches were first tested for effects on proliferation of WT MuSC and batches without efficacy were discarded. For Akt-inhibitor experiments, MuSCs were directly plated in growth medium containing 0.1μM of Akt inhibitor (MK-2206, Selleckchem, # S1078) or equal amount of vehicle (DMSO) and 2 hours after plating, 8μg/mL of human recombinant WISP1 protein (Peprotech, # 120-18) or equal amount of vehicle were added to the medium. The medium was thereafter changed daily using fresh WISP1 and Akt-inhibitor. MuSCs were grown for 3 days and 1μM EdU was added to the medium 3 hours before fixing the cells. For FAP clonal assay, FAPs were directly plated in Matrigel-coated 96 well plates at 1 cell per well in growth medium and grown for 3 weeks with medium change every 3 days.

Myoblast culture and western blot.—Human Skeletal Muscle Cells (Lonza, # LZ-CC-2580) were plated on fibronectin-coated 6 wells plate at a density of 100 000 cells per well. Cells were grown for 48h in Skeletal Muscle Cell Growth Medium (AmsBio, SKM-M medium). Cells were treated with WISP1 by adding 8μg/mL of human recombinant WISP1

protein (Peprotech, # 120-18) in medium that was exchanged daily. Proteins were extracted in RIPA lysis and extraction buffer (Thermofisher, #89901) supplemented with protease and phosphatase inhibitor cocktail (ThermoFisher, #78446). Protein concentration was determined by a BCA assay (Pierce), and samples were diluted at 1.3 ug/mL and boiled 5 min in Laemmli buffer. Samples were run on 4–12% Bis-Tris Protein gels (Novex, # BN1003) and then transferred using the wet system from Life Technologies. Antibodies used were phospho-Akt (Ser473) Antibody (Cell Signaling, #4060, 1/1000), Akt Antibody (Cell Signaling, #9272, 1/1000) and GAPDH (Cell Signaling, #5174, 1/1000).

Immunocytochemistry and image analysis.—EdU incorporation was revealed using the Click-iT assay (Molecular Probes) according to manufacturer's instruction. Briefly, cells were fixed during 15 minutes in 4% PFA, permeabilized during 20 minutes in PBTX 0.5%, stained with the Click-iT reaction mix and counterstained with DAPI. For MyHC staining, cells were fixed during 10 minutes in 4% PFA, permeabilized using cold EtOH/MetOH (v/v) during 5 min, incubated during 1h with the primary antibody anti-MHC 1/200 (Millipore clone A4.1025) in PBS, 1% Horse Serum at room temperature, and incubated during 30min with the secondary antibody Alexa488 anti-mouse IgG diluted at 1/1000 (Life Tech. A-10680) and Hoeschst 33342 in PBS, 1% Horse Serum at room temperature. For Pax7 and MyoD immunostaining, cells were blocked for 1–2 h in 5% goat serum, 1% BSA and 0.2% PBTX, before incubation with primary mouse anti-mouse Pax7 (DHSB, purified, 2.5 μg/ml), rabbit-anti mouse MyoD antibody (Santa-Cruz #sc-304, 1/100) and secondary antibodies. For α-SMA staining used to asses fibrogenic conversion, FAPs were fixed and permeabilized, blocked in PBS, 5% GS, 1% BSA, and incubated with a mouse IgG2a anti-mouse α-smooth muscle actin antibody (#Sigma A5228, 1/150). For collagen1a1 staining, cells were fixed 10min with 4% PFA, permeabilized 10min with PBS 0.5% Triton X-100 and blocked overnight at 4°C in PBS 5% NGS, 1% BSA. The primary Col1a1 antibody and the secondary antibody were successively incubated 2h at room temperature in PBS 5% NGS, 1% BSA at dilutions of 1/200 and 1/1000, respectively. For adipogenic differentiation, cells were fixed for 10 minutes in PFA 4%, then incubated with Bodipy 493/503 (LifeTechnologies, 1/1000 of the 1mg/ml stock solution of bodipy in ethanol), and counterstained with Hoechst 33342. Image acquisition was performed using the ImageXpress (Molecular Devices) platform. Quantifications were done with the MetaXpress software using the Multi-Wavelength Cell Scoring or Cell Scoring application modules, or an automated image processing algorithm developed internally.

Quantification of asymmetric MuSC divisions.—Single myofibers were isolated and cultured ex vivo from the EDL muscles of Myf5-Cre/ROSA26-YFP uninjured mice as described above. Myofibers were cultured for 42h in DMEM media with 15% FBS and 1% chick embryo extract (Accurate Chemicals) and treated with 8 μg/mL of mouse recombinant WISP1 protein or vehicle. After 42h, myofibers were fixed with PFA 2%/PBS 1× for 10min at room temperature and then washed 3 times in PBS for 5 min. Myofibers were then permeabilized for 10min with 0.1% Triton X-100, 0.1M Glycine in PBS 1× and followed by blocking solution for 2h at room temperature with 5% horse serum, 2% BSA, 0.1% Triton X-100 in PBS 1×. Incubation with undiluted anti-Pax7 (DHSB) and anti-GFP (1:1000) primary antibodies was performed overnight. The next day, day myofibers were washed 3

times in PBS for 5 min and incubated with anti-mouse IgG1 and anti-chicken IgG secondary antibodies in PBS for 1h at room temperature. Finally, myofibers were mounted with mounting medium containing Hoechst (10uL of Hoechst 1ug/uL). MuSCs divisions were quantified based on the expression or absence of YFP on Pax7+ doublets ($Pax7^+/YFP^-$-$Pax7^+/YFP^+$ asymmetric or $Pax7^+/YFP^-$-$Pax7^+/YFP^-$ symmetric). Quantifications were done manually using an epifluorescent microscope Zeiss AxioObserver Z1. Digital images were taking using the same microscope.

Immunofluorescence and image analysis.—TA muscles were frozen in isopentane cooled with liquid nitrogen, and further sectioned at 10μm using a cryostat. Hematoxylin and Eosin (H&E) staining was performed by placing the dried slides in Harris-hematoxylin during 1min, followed by differentiation in 1% acid-alcohol and washing, and 1min bath in eosine-phloxine (10g/L). Oil-Red-O staining was performed on air-dried slides by incubating them in 50% ethanol during 30min, followed by 15min incubation in 2.5g/L oil-red-O solution in 70% ethanol, 1 min washing in 50% ethanol then water; and slides were counterstained with Mayer's hematoxylin. For laminin-eMHC immunostaining, cryosections were allowed to dry for 10 minutes and blocked for 45 minutes at room temperature in blocking solution (PBS, 4% BSA, 1% FBS). Cryosections were stained for 3 hours at room temperature using monoclonal anti-laminin antibody produced in rabbit (Sigma-Aldrich #L9393) and anti-eMHC produced in mouse (DSHB, #F1.652) diluted at 1/100 and 1/500 in the blocking solution, respectively. For perilipin staining, sections were fixed during 10 minutes with PFA 4%, permeabilized during 10 minutes in PBTX 0,5%, blocked in PBS, 4% Goat-serum. A rabbit polyclonal anti-mouse perilipin antibody (Sigma #P1873) and a chicken polyclonal anti-human laminin antibody (Life Span Bioscience #LC-C96142-100) were then incubated on the sections during 3h at room temperature, diluted 1/300 and 1/200 in the blocking solution, respectively. Slides were then incubated during 1 hour at room temperature with secondary antibodies and counterstained with Hoechst 33342. For Pax7, MyoD and Ki67 stainings, slides were fixed with PFA 4%, and permeabilized in cold methanol. Antigen retrieval was performed with two successive incubations of hot citric acid 0.01M pH6 during 10min, and sections were further blocked in PBS, 4% BSA during 3h, followed by 30 minutes blocking with a goat-anti-mouse FAB diluted 1/50 (Jackson #115-007-003). Mouse anti-mouse Pax7 (DHSB, purified), rabbit-anti mouse MyoD antibody (Santa-Cruz #sc-304 or Abcam # ab198251), rabbit-anti mouse Ki67 (Abcam #ab15580) and chicken anti-human laminin (Life Span Bioscience #LC-C96142-100) antibodies were used at 2.5 μg/ml, 1/100, 1/100 and 1/200 in blocking solution, respectively. Pax7 signal was further amplified using a goat-anti mouse IgG1-biotin (1/1000, Jackson ImmunoResearch #115-065-205) followed by a Streptavidin Alexa555 (1/2000) (Life Tech. S-21381) treatment, together with other secondary antibodies and Hoechst counterstain. Stained tissues were imaged using an Olympus VS120 slide scanner or a Leica DMI 4000B microscope and analyzed either using the VS-ASW FL software measurement tools or the LAS AF software. The number of Pax7, MyoD and Ki67 positive cells was determined manually by counting of immunostainings in muscle sections in random areas of the injured region, and the area covered by eMHC-positive fibers and degenerated area was determined manually across the entire sections. For FAP transplantation experiments, the quantification of Pax7 and MyoD immunostainings was restricted to the regenerating regions surrounding

the sites of injection identified by the fluorescent beads (ThermoFischer #F8826). The size of myofibers with centralized nuclei was calculated from laminin/DAPI stainings on all fibers of the section, and Oil-Red-O positive structures segmentation and area determination were performed across the entire sections, using an automated image processing algorithm developed internally using the MetaXpress software (Molecular Devices). For FAP staining, 8μm cryosections were labeled with antibodies against PDGFRα overnight at 4°C and Laminin counter-staining was performed for 2h at 37°C. Secondary antibodies were coupled to FITC and Cy3. Images were recorded with a DMI 6000 Leica microscope connected to a Coolsnap camera at 20× magnification. For each condition of each experiment, at least 8-10 fields chosen randomly were counted. The number of labeled PDGFRα$^+$ cells was calculated using the cell tracker in ImageJ.

Masson Trichrome staining.—Frozen sections were dried and fixed 1h with 4% PFA and then incubated overnight in Bouin solution. Slides were rinsed in water for 1min and stained in Weigert solution for 5 min. Slides were successively dipped in water for 1 min, 1% HCl diluted in 100% Ethanol for 3 sec, again for 10 min in water and in 1% acetic acid for 1 min. Slides were then stained in 1% Biebrich scarlet-acid fuchsin solution for 5 min. Slides were successively incubated in 1% acetic acid for 2 min, 5% phosphomolybdic-phosphotungstic acid solution for 10min and in 1% acetic acid for 2 min. Slides were stained in 3% Aniline blue for 5 min and differentiated in 1% acetic acid for 2min. Finally, slides were dehydrated in Ethanol 100% for 2 min and cleared in Xylene for 2 min before being mounted with Eukitt mounting medium.

RNA fluorescent *in-situ* hybridization (RNA-FISH).—Frozen muscle samples were sectioned using a cryo-microtome (Leica-1850 UV) and *Wisp1*-mRNA expression in muscle cross sections was analyzed using the ViewRNA ISH Tissue Assay Kit and Fast red substrate following the manufacturer's instructions (ThermoFisher Scientific, USA). Wisp1 was detected using the VIEWRNA type-1 probe-set for Mus musculus *Wisp-1* (VB1-10640) and nuclei were detected with DAPI. Images were acquired using an Olympus-VS120 slide scanner. Image overlay with Pax7 was performed by merging the RNA FISH and Pax7 immunofluorescence on adjacent serial sections and overlapping morphological structures and selected DAPI-positive nuclei.

Transcriptomic analysis.—RNA was extracted from freshly sorted MuSCs and FAPs using the RNeasy Micro Kit (Qiagen). RNA samples were quality controlled and then subjected to 3' microarray analysis on Illumina MouseRef–8_V2 chips. 3ng of total RNA were used to produce cRNA in a two-round amplification protocol, using first Messageamp II aRNA amplification kit (AM1751, Life Technologies, Inc.) followed by Messageamp II–biotin enhanced aRNA amplification kit (AM1791, Life Technologies, Inc.). 750ng of cRNA were hybridized for 16h at 55°C on Illumina MouseRef–8 v2 microarrays. Quality of total RNA was checked by using the Bioanalyzer 2100 with Total RNA Pico kit, and quality of cRNA was checked by using the Bioanalyzer 2100 with the Total RNA Nano kit (Agilent Technologies). Quantifications were done using the Quant-iT RiboGreen RNA Assay Kit (Life Technologies, Inc.). Illumina expression signals were quantile-normalized. We applied a nonspecific filter to discard probes with low variability and retained 12,848 Illumina probe

whose standard deviation was greater than the median of the s.d. of all of the probe. For differential expression analysis and pathway analyses, genes (represented by probes) were tested for differential expression using the moderated t-statistic as implemented in LIMMA44 for both data sets. Venn diagrams where built from differentially expressed genes (http://www.cmbi.ru.nl/cdd/biovenn/index.php)(Hulsen et al., 2008). We used the Pantherdb platform to identify protein classes (signaling molecules) within lists of differentially expressed genes (http://pantherdb.org/).

Quantitative PCR.—RNA was extracted from frozen muscles or freshly sorted cells using miRNeasy Mini Kit or RNeasy Micro Kit (Qiagen), respectively. RNA samples were subjected to reverse transcription using random primers (High Capacity cDNA Reverse Transcription Kit, ABI). Quantitative PCR on full muscle was performed using the SYBR Green I master kit (Roche) on a LightCycler 480. Reference genes (ATP5b, EIF2a and PSMB4) were selected based on their stability across time points of regeneration from micro-array data. Quantification of PDGFRα variants both in full muscles and freshly isolated FAPs were performed using the SYBR Green method, and primers amplifying the intronic variant number 16 were designed as previously described (PDGFRα In) (Mueller et al., 2016). Other qPCR reactions performed using SYBR assays were performed with the following primers (5’3’): ATP5b forward: ACCTCGGTGCAGGCTATCTA; ATP5b reverse: AATAGCCCGGGACAACACAG; CD11b forward: GCCTGTGAAGTACGCCATCT; CD11b reverse: GCCCAGGTTGTTGAACTGGT; CD11c forward: ACACTGAGTGATGCCACTGT; CD11c reverse: TTCGGAGGTCACCTAGTTGGG; CD31 forward: CACACCGAGAGCTACGTCAT; CD31 reverse: TTGGATACGCCATGCACCTT; EIF2a forward: CACGGTGCTTCCCAGAGAAT; EIF2a reverse: TGCAGTAGTCCCTTGTTAGCG; F4/80 forward: CTCTTCTGGGGCTTCAGTGG; F4/80 reverse: TGTCAGTGCAGGTGGCATAA; PSMB4 forward: GCGAGTCAACGACAGCACTA; PSMB4 reverse: TCATCAATCACCATCTGGCCG; Pax7 forward: AAGTTCGGGAAGAAAGAGGACGAC; Pax7 reverse: GAGGTCGGGTTCTGATTCCACATC; MyoD forward: GCAGATGCACCACCAGAGTC; MyoD reverse: GCACCTGATAAATCGCATTGG; Myog forward: GTGCCCAGTGAATGCAACTC; Myog reverse: CGCGAGCAAATGATCTCCTG; PDGFRα In forward: AAAAGTGCCCATGCTCATTC; PDGFRα In reverse: GCTTGGCAGAGCTACCTGTC; PDGFRα FL forward: AGTGGCTACATCATCCCCCT; PDGFRα FL reverse: CCGAAGTCTGTGAGCTGTGT; TCF4 forward: GGCGATGAGAACCTGCAAGA; TCF4 reverse: GGTCCTCATCATCGTTATTGCTAGA; WISP1 forward: CAGTGAGCCCAAGAGTCAGG; WISP1 reverse: TCGTCTCTGTCAGCTTGCAC; WISP1 forward (for KO experiment): ATCGCCCGAGGTACGCAATAGG; WISP1 reverse (for KO experiment): CAGCCCACCGTGCCATCAATG; PDGFRα forward: AGTGGCTACATCATCCCCCT; PDGFRα reverse: CCGAAGTCTGTGAGCTGTGT. Quantitative PCRs on isolated progenitors was performed using Taqman probes (ABI) on a LightCycler 480. Reference genes (Ap1m1 and Ywhaq) were selected based on their stability across cell types and states from micro-array data. Taqman probes used for real-time PCR were mWISP1 (ThermoFisher Scientific, Mm01200484_m1, #4331182), mAp1m1 (ThermoFisher

Scientific, Mm00475912_m1, #4448489) and mYwhaq (ThermoFisher Scientific, Mm01231061_g1, #4448489).

Protein expression by slow off-rate modified aptamer assay.—Muscle samples were pulverized using the cryoPREP impactor system (Covaris). The muscle powder was then subjected to mechanical lysis using a Polytron homogenizer and proteins were extracted in 50 mM Tris (pH 7.5), 150 mM NaCl, 50 mM NaF, 1 mM EDTA, 0.5% TritonX. Protein concentration was determined by a BCA assay and samples were diluted at 250ug/mL. Protein extracts were analyzed using DNA aptamer-based recognition on the SOMAscan platform (Somalogic, Boulder, CO, USA). Median normalized relative fluorescence units (RFU) were log2 transformed before applying principal component analysis and linear models. Statistical analyses were performed in R 3.1.3.

QUANTIFICATION AND STATISTICAL ANALYSIS

All mice were randomized according to body weight before interventions. Sample size determination was based on the expected effect size and variability that was previously observed for similar readouts in the investigators' labs. In vivo treatments were not blinded, but imaging readouts were analyzed in a blinded manner. Genome-wide statistical analyses and Kolmogorov–Smirnov tests were performed using R version 3.1.3 and relevant Bioconductor packages. GO terms were tested on genes differentially expressed in the indicated conditions using a Benjamini-Hochberg adjusted p-value< 0.05. Genes upregulated during FAP activation were filtered as: Benjamini-Hochberg adjusted p-value < 0.001, Fold-change > 2. Genes differentially upregulated in FAPs during activation with age were filtered as: Benjamini-Hochberg adjusted p-value [Activation young] < 0.001, Fold-change [Activation young] > 2; Benjamini-Hochberg adjusted p-value [interaction: Activation*Age] < 0.25; Benjamini-Hochberg adjusted p-value [aged activated FAPs vs. young activated FAPs] < 0.1. All other statistical analyses were performed using GraphPad Prism (GraphPad Software). Statistical significance for binary comparisons was assessed by a Mann-Whitney test. All exploratory and signaling experiments were analyzed by using two-tailed tests. For comparison of more than two groups, one-way or two-way ANOVAs were used, according to the experimental design, and followed by Bonferroni multiple-comparison testing. Comparison of distributions were performed by a Kolmogorov-Smirnov test. All data are expressed as mean + s.e.m.

DATA AND SOFTWARE AVAILABILITY

The genomics data from this study have been submitted to the NCBI Gene Expression Omnibus (GEO) (http://www.ncbi.nlm.nih.gov/geo) under accession numbers GSE92508 and GSE81096. All software used were freely or commercially available.

Supplementary Material

Refer to Web version on PubMed Central for supplementary material.

Acknowledgements

We thank Marian Young (National Institute of Dental and Craniofacial Research, NIH, Bethesda) for sharing WISP1−/− mice and Edward Schmidt (Montana State University) for advices on the use of TdTomato mice. We are grateful to J. Sanchez (NIHS) for help with mouse husbandry and to the NIHS community for fruitful discussions and support. This work was funded by Nestec. O.M., J.N.F. and C.F.B are supported by the Fondation Suisse de Recherche sur les Maladies Musculaires (FSRMM). C.F.B. is supported by the Natural Sciences and Engineering Research Council of Canada (NSERC), the Fonds de recherche du Québec – Santé (FRQS), the ThéCell Network (supported by the FRQS), the Canadian Stem Cell Network, the CHUS Foundation, the Banting Research Foundation, and a Research Chair of the Centre de recherche medicale de l'Université de Sherbrooke (CRMUS). M.A.R. holds the Canada Research Chair in Molecular Genetics. The studies from the laboratory of M.A.R. were carried out with support of grants from the US National Institutes for Health [R01AR044031], the Canadian Institutes for Health Research [FDN-148387], the Muscular Dystrophy Association, and the Stem Cell Network.

References

Addison O, Marcus RL, Lastayo PC, and Ryan AS (2014). Intermuscular fat: a review of the consequences and causes. Int J Endocrinol 2014, 309570. [PubMed: 24527032]

Almada AE, and Wagers AJ (2016). Molecular circuitry of stem cell fate in skeletal muscle regeneration, ageing and disease. Nat Rev Mol Cell Biol 17, 267–279. [PubMed: 26956195]

Bentzinger CF, Wang YX, von Maltzahn J, Soleimani VD, Yin H, and Rudnicki MA (2013). Fibronectin regulates Wnt7a signaling and satellite cell expansion. Cell Stem Cell 12, 75–87. [PubMed: 23290138]

Bernet JD, Doles JD, Hall JK, Kelly Tanaka K, Carter TA, and Olwin BB (2014). p38 MAPK signaling underlies a cell-autonomous loss of stem cell self-renewal in skeletal muscle of aged mice. Nat Med 20, 265–271. [PubMed: 24531379]

Blau HM, Cosgrove BD, and Ho AT (2015). The central role of muscle stem cells in regenerative failure with aging. Nat Med 21, 854–862. [PubMed: 26248268]

Brack AS, Conboy MJ, Roy S, Lee M, Kuo CJ, Keller C, and Rando TA (2007). Increased Wnt signaling during aging alters muscle stem cell fate and increases fibrosis. Science 317, 807–810. [PubMed: 17690295]

Brack AS, and Munoz-Canoves P (2015). The ins and outs of muscle stem cell aging. Skelet Muscle 6, 1.

Brun CE, Wang YX, and Rudnicki MA (2018). Single EDL Myofiber Isolation for Analyses of Quiescent and Activated Muscle Stem Cells. Methods Mol Biol 1686, 149–159. [PubMed: 29030819]

Carlson ME, Hsu M, and Conboy IM (2008). Imbalance between pSmad3 and Notch induces CDK inhibitors in old muscle stem cells. Nature 454, 528–532. [PubMed: 18552838]

Chakkalakal JV, Jones KM, Basson MA, and Brack AS (2012). The aged niche disrupts muscle stem cell quiescence. Nature 490, 355–360. [PubMed: 23023126]

Cosgrove BD, Gilbert PM, Porpiglia E, Mourkioti F, Lee SP, Corbel SY, Llewellyn ME, Delp SL, and Blau HM (2014). Rejuvenation of the muscle stem cell population restores strength to injured aged muscles. Nat Med 20, 255–264. [PubMed: 24531378]

Elabd C, Cousin W, Upadhyayula P, Chen RY, Chooljian MS, Li J, Kung S, Jiang KP, and Conboy IM (2014). Oxytocin is an age-specific circulating hormone that is necessary for muscle maintenance and regeneration. Nat Commun 5, 4082. [PubMed: 24915299]

Fiore D, Judson RN, Low M, Lee S, Zhang E, Hopkins C, Xu P, Lenzi A, Rossi FM, and Lemos DR (2016). Pharmacological blockage of fibro/adipogenic progenitor expansion and suppression of regenerative fibrogenesis is associated with impaired skeletal muscle regeneration. Stem Cell Res 17, 161–169. [PubMed: 27376715]

Fry CS, Kirby TJ, Kosmac K, McCarthy JJ, and Peterson CA (2016). Myogenic Progenitor Cells Control Extracellular Matrix Production by Fibroblasts during Skeletal Muscle Hypertrophy. Cell Stem Cell.

Garcia-Prat L, Martinez-Vicente M, Perdiguero E, Ortet L, Rodriguez-Ubreva J, Rebollo E, Ruiz-Bonilla V, Gutarra S, Ballestar E, Serrano AL, et al. (2016). Autophagy maintains stemness by preventing senescence. Nature 529, 37–42. [PubMed: 26738589]

Heredia JE, Mukundan L, Chen FM, Mueller AA, Deo RC, Locksley RM, Rando TA, and Chawla A (2013). Type 2 innate signals stimulate fibro/adipogenic progenitors to facilitate muscle regeneration. Cell 153, 376–388. [PubMed: 23582327]

Hulsen T, de Vlieg J, and Alkema W (2008). BioVenn - a web application for the comparison and visualization of biological lists using area-proportional Venn diagrams. BMC Genomics 9, 488. [PubMed: 18925949]

Ikemoto-Uezumi M, Uezumi A, Tsuchida K, Fukada S, Yamamoto H, Yamamoto N, Shiomi K, and Hashimoto N (2015). Pro-Insulin-Like Growth Factor-II Ameliorates Age-Related Inefficient Regenerative Response by Orchestrating Self-Reinforcement Mechanism of Muscle Regeneration. Stem Cells 33, 2456–2468. [PubMed: 25917344]

Joe AW, Yi L, Natarajan A, Le Grand F, So L, Wang J, Rudnicki MA, and Rossi FM (2010). Muscle injury activates resident fibro/adipogenic progenitors that facilitate myogenesis. Nat Cell Biol 12, 153–163. [PubMed: 20081841]

Konigshoff M, Kramer M, Balsara N, Wilhelm J, Amarie OV, Jahn A, Rose F, Fink L, Seeger W, Schaefer L, et al. (2009). WNT1-inducible signaling protein-1 mediates pulmonary fibrosis in mice and is upregulated in humans with idiopathic pulmonary fibrosis. J Clin Invest 119, 772–787. [PubMed: 19287097]

Kuang S, Kuroda K, Le Grand F, and Rudnicki MA (2007). Asymmetric self-renewal and commitment of satellite stem cells in muscle. Cell 129, 999–1010. [PubMed: 17540178]

Kuswanto W, Burzyn D, Panduro M, Wang KK, Jang YC, Wagers AJ, Benoist C, and Mathis D (2016). Poor Repair of Skeletal Muscle in Aging Mice Reflects a Defect in Local, Interleukin-33-Dependent Accumulation of Regulatory T Cells. Immunity 44, 355–367. [PubMed: 26872699]

Lafont J, Thibout H, Dubois C, Laurent M, and Martinerie C (2005). NOV/CCN3 induces adhesion of muscle skeletal cells and cooperates with FGF2 and IGF-1 to promote proliferation and survival. Cell Commun Adhes 12, 41–57. [PubMed: 16371345]

Lemos DR, Babaeijandaghi F, Low M, Chang CK, Lee ST, Fiore D, Zhang RH, Natarajan A, Nedospasov SA, and Rossi FM (2015). Nilotinib reduces muscle fibrosis in chronic muscle injury by promoting TNF-mediated apoptosis of fibro/adipogenic progenitors. Nat Med 21, 786–794. [PubMed: 26053624]

Liu W, Liu Y, Lai X, and Kuang S (2012). Intramuscular adipose is derived from a non-Pax3 lineage and required for efficient regeneration of skeletal muscles. Dev Biol 361, 27–38. [PubMed: 22037676]

Lukjanenko L, Brachat S, Pierrel E, Lach-Trifilieff E, and Feige JN (2013). Genomic profiling reveals that transient adipogenic activation is a hallmark of mouse models of skeletal muscle regeneration. PLoS One 8, e71084. [PubMed: 23976982]

Lukjanenko L, Jung MJ, Hegde N, Perruisseau-Carrier C, Migliavacca E, Rozo M, Karaz S, Jacot G, Schmidt M, Li L, et al. (2016). Loss of fibronectin from the aged stem cell niche affects the regenerative capacity of skeletal muscle in mice. Nat Med 22, 897–905. [PubMed: 27376579]

Maeda A, Ono M, Holmbeck K, Li L, Kilts TM, Kram V, Noonan ML, Yoshioka Y, McNerny EM, Tantillo MA, et al. (2015). WNT1-induced Secreted Protein-1 (WISP1), a Novel Regulator of Bone Turnover and Wnt Signaling. J Biol Chem 290, 14004–14018. [PubMed: 25864198]

Maiese K (2014). WISP1: Clinical insights for a proliferative and restorative member of the CCN family. Curr Neurovasc Res 11, 378–389. [PubMed: 25219658]

Mann CJ, Perdiguero E, Kharraz Y, Aguilar S, Pessina P, Serrano AL, and Munoz-Canoves P (2011). Aberrant repair and fibrosis development in skeletal muscle. Skelet Muscle 1, 21. [PubMed: 21798099]

Mashinchian O, Pisconti A, Le Moal E, and Bentzinger CF (2018). The Muscle Stem Cell Niche in Health and Disease. Curr Top Dev Biol 126, 23–65. [PubMed: 29305000]

Messina S, Mazzeo A, Bitto A, Aguennouz M, Migliorato A, De Pasquale MG, Minutoli L, Altavilla D, Zentilin L, Giacca M, et al. (2007). VEGF overexpression via adeno-associated virus gene transfer promotes skeletal muscle regeneration and enhances muscle function in mdx mice. FASEB J 21, 3737–3746. [PubMed: 17575261]

Mozzetta C, Consalvi S, Saccone V, Tierney M, Diamantini A, Mitchell KJ, Marazzi G, Borsellino G, Battistini L, Sassoon D, et al. (2013). Fibroadipogenic progenitors mediate the ability of HDAC

inhibitors to promote regeneration in dystrophic muscles of young, but not old Mdx mice. EMBO Mol Med 5, 626–639. [PubMed: 23505062]

Mueller AA, van Velthoven CT, Fukumoto KD, Cheung TH, and Rando TA (2016). Intronic polyadenylation of PDGFRalpha in resident stem cells attenuates muscle fibrosis. Nature 540, 276–279. [PubMed: 27894125]

Murahovschi V, Pivovarova O, Ilkavets I, Dmitrieva RM, Docke S, Keyhani-Nejad F, Gogebakan O, Osterhoff M, Kemper M, Hornemann S, et al. (2015). WISP1 is a novel adipokine linked to inflammation in obesity. Diabetes 64, 856–866. [PubMed: 25281430]

Murphy MM, Lawson JA, Mathew SJ, Hutcheson DA, and Kardon G (2011). Satellite cells, connective tissue fibroblasts and their interactions are crucial for muscle regeneration. Development 138, 3625–3637. [PubMed: 21828091]

Naito AT, Sumida T, Nomura S, Liu ML, Higo T, Nakagawa A, Okada K, Sakai T, Hashimoto A, Hara Y, et al. (2012). Complement C1q activates canonical Wnt signaling and promotes aging-related phenotypes. Cell 149, 1298–1313. [PubMed: 22682250]

Nishida T, Kondo S, Maeda A, Kubota S, Lyons KM, and Takigawa M (2009). CCN family 2/connective tissue growth factor (CCN2/CTGF) regulates the expression of Vegf through Hif-1alpha expression in a chondrocytic cell line, HCS-2/8, under hypoxic condition. Bone 44, 24–31. [PubMed: 18835464]

Ono M, Masaki A, Maeda A, Kilts TM, Hara ES, Komori T, Pham H, Kuboki T, and Young MF (2018). CCN4/WISP1 controls cutaneous wound healing by modulating proliferation, migration and ECM expression in dermal fibroblasts via alpha5beta1 and TNFalpha. Matrix Biol.

Pagano AF, Demangel R, Brioche T, Jublanc E, Bertrand-Gaday C, Candau R, Dechesne CA, Dani C, Bonnieu A, Py G, et al. (2015). Muscle Regeneration with Intermuscular Adipose Tissue (IMAT) Accumulation Is Modulated by Mechanical Constraints. PLoS One 10, e0144230. [PubMed: 26629696]

Price FD, von Maltzahn J, Bentzinger CF, Dumont NA, Yin H, Chang NC, Wilson DH, Frenette J, and Rudnicki MA (2014). Inhibition of JAK-STAT signaling stimulates adult satellite cell function. Nat Med 20, 1174–1181. [PubMed: 25194569]

Prigge JR, Wiley JA, Talago EA, Young EM, Johns LL, Kundert JA, Sonsteng KM, Halford WP, Capecchi MR, and Schmidt EE (2013). Nuclear double-fluorescent reporter for in vivo and ex vivo analyses of biological transitions in mouse nuclei. Mamm Genome 24, 389–399.

Quiros M, Nishio H, Neumann PA, Siuda D, Brazil JC, Azcutia V, Hilgarth R, O'Leary MN, Garcia-Hernandez V, Leoni G, et al. (2017). Macrophage-derived IL-10 mediates mucosal repair by epithelial WISP-1 signaling. J Clin Invest 127, 3510–3520. [PubMed: 28783045]

Raggi C, and Berardi AC (2012). Mesenchymal stem cells, aging and regenerative medicine. Muscles Ligaments Tendons J 2, 239–242. [PubMed: 23738303]

Rozo M, Li L, and Fan CM (2016). Targeting beta1-integrin signaling enhances regeneration in aged and dystrophic muscle in mice. Nat Med 22, 889–896. [PubMed: 27376575]

Schworer S, Becker F, Feller C, Baig AH, Kober U, Henze H, Kraus JM, Xin B, Lechel A, Lipka DB, et al. (2016). Epigenetic stress responses induce muscle stem-cell ageing by Hoxa9 developmental signals. Nature 540, 428–432. [PubMed: 27919074]

Shefer G, Van de Mark DP, Richardson JB, and Yablonka-Reuveni Z (2006). Satellite-cell pool size does matter: defining the myogenic potency of aging skeletal muscle. Dev Biol 294, 50–66. [PubMed: 16554047]

Sousa-Victor P, Gutarra S, Garcia-Prat L, Rodriguez-Ubreva J, Ortet L, Ruiz-Bonilla V, Jardi M, Ballestar E, Gonzalez S, Serrano AL, et al. (2014). Geriatric muscle stem cells switch reversible quiescence into senescence. Nature 506, 316–321. [PubMed: 24522534]

Tallquist MD, Weismann KE, Hellstrom M, and Soriano P (2000). Early myotome specification regulates PDGFA expression and axial skeleton development. Development 127, 5059–5070. [PubMed: 11060232]

Tchkonia T, Morbeck DE, Von Zglinicki T, Van Deursen J, Lustgarten J, Scrable H, Khosla S, Jensen MD, and Kirkland JL (2010). Fat tissue, aging, and cellular senescence. Aging Cell 9, 667–684. [PubMed: 20701600]

Tierney MT, Stec MJ, Rulands S, Simons BD, and Sacco A (2018). Muscle Stem Cells Exhibit Distinct Clonal Dynamics in Response to Tissue Repair and Homeostatic Aging. Cell Stem Cell 22, 119–127 e113. [PubMed: 29249462]

Uezumi A, Fukada S, Yamamoto N, Takeda S, and Tsuchida K (2010). Mesenchymal progenitors distinct from satellite cells contribute to ectopic fat cell formation in skeletal muscle. Nat Cell Biol 12, 143–152. [PubMed: 20081842]

Varga T, Mounier R, Horvath A, Cuvellier S, Dumont F, Poliska S, Ardjoune H, Juban G, Nagy L, and Chazaud B (2016). Highly Dynamic Transcriptional Signature of Distinct Macrophage Subsets during Sterile Inflammation, Resolution, and Tissue Repair. J Immunol 196, 4771–4782. [PubMed: 27183604]

Verma M, Asakura Y, Murakonda BSR, Pengo T, Latroche C, Chazaud B, McLoon LK, and Asakura A (2018). Muscle Satellite Cell Cross-Talk with a Vascular Niche Maintains Quiescence via VEGF and Notch Signaling. Cell Stem Cell 23, 530–543 e539. [PubMed: 30290177]

Vinel C, Lukjanenko L, Batut A, Deleruyelle S, Pradere JP, Le Gonidec S, Dortignac A, Geoffre N, Pereira O, Karaz S, et al. (2018). The exerkine apelin reverses age-associated sarcopenia. Nat Med 24, 1360–1371. [PubMed: 30061698]

Wang Y, Wehling-Henricks M, Samengo G, and Tidball JG (2015). Increases of M2a macrophages and fibrosis in aging muscle are influenced by bone marrow aging and negatively regulated by muscle-derived nitric oxide. Aging Cell 14, 678–688. [PubMed: 26009878]

Wright LH, Herr DJ, Brown SS, Kasiganesan H, and Menick DR (2018). Angiokine Wisp-1 is increased in myocardial infarction and regulates cardiac endothelial signaling. JCI Insight 3.

Xu M, Palmer AK, Ding H, Weivoda MM, Pirtskhalava T, White TA, Sepe A, Johnson KO, Stout MB, Giorgadze N, et al. (2015). Targeting senescent cells enhances adipogenesis and metabolic function in old age. Elife 4, e12997. [PubMed: 26687007]

Yoshioka Y, Ono M, Maeda A, Kilts TM, Hara ES, Khattab H, Ueda J, Aoyama E, Oohashi T, Takigawa M, et al. (2016). CCN4/WISP-1 positively regulates chondrogenesis by controlling TGF-beta3 function. Bone 83, 162–170. [PubMed: 26555637]

Zhang H, Ryu D, Wu Y, Gariani K, Wang X, Luan P, D'Amico D, Ropelle ER, Lutolf MP, Aebersold R, et al. (2016). NAD(+) repletion improves mitochondrial and stem cell function and enhances life span in mice. Science 352, 1436–1443. [PubMed: 27127236]

Highlights:

- Aging alters the myogenic support of FAPs to MuSCs
- Aged FAPs produce less matricellular WISP1
- FAP-derived WISP1 is required for MuSC expansion and commitment
- Restoring WISP1 levels rejuvenates the myogenic potential of aged MuSCs

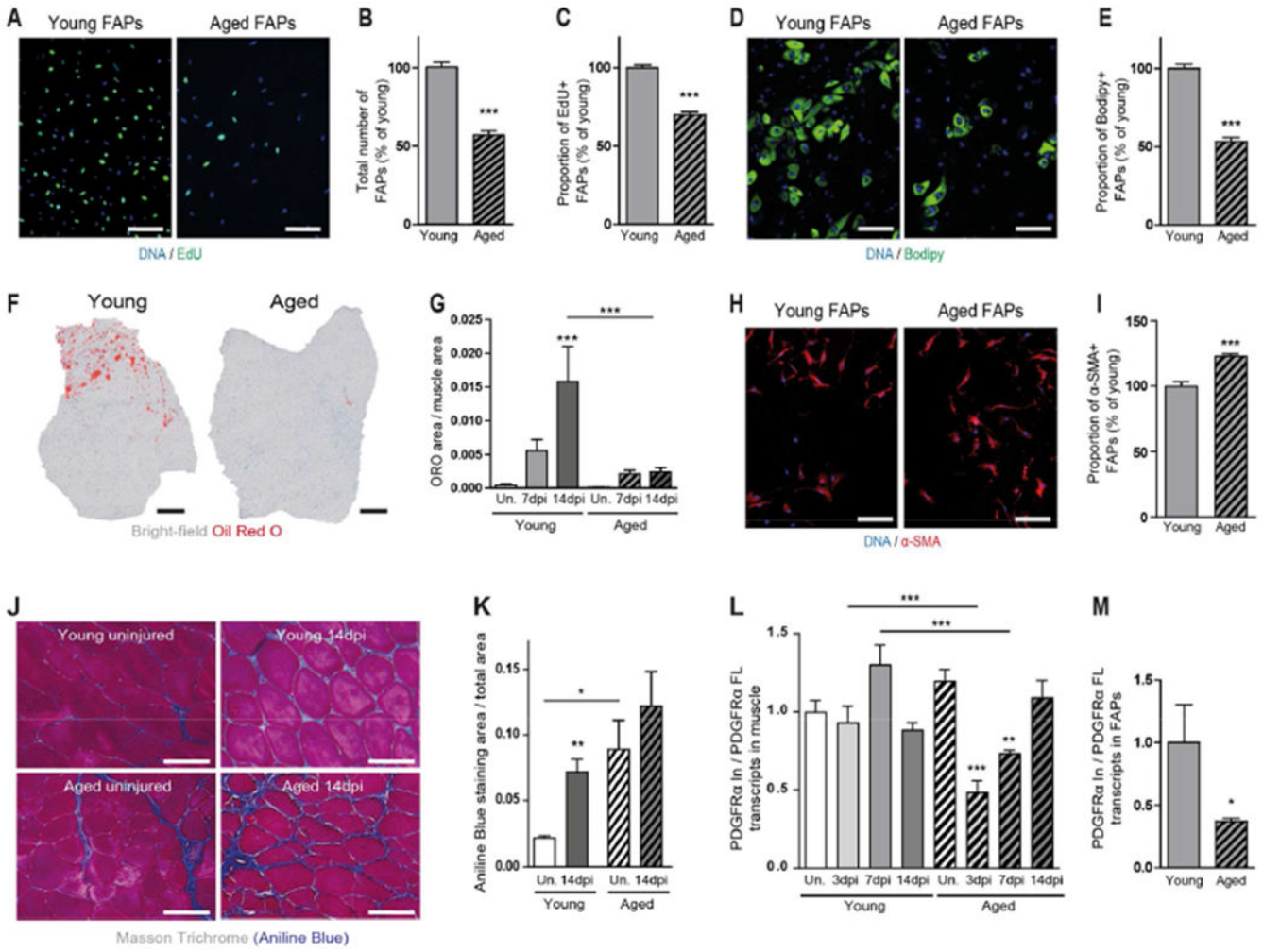

Figure 1. Aging Impairs FAP Function and Uncouples Adipogenic from Fibrogenic Fate Decisions

(A) Representative images of cell numbers and EdU incorporation of FAPs 6 days (d) after isolation from uninjured muscles of young or aged mice. Scale bars = 100 μm. (B) Quantification of the number of FAPs 6 d after isolation from uninjured muscles of young or aged mice. (C) Quantification of the percentage of EdU+ FAPs 6 d after isolation from young and aged uninjured muscles. (D) Representative images of FAPs differentiated under pro-adipogenic conditions 13 d after isolation from uninjured muscles of young or aged mice. Lipid droplets were detected by bodipy staining. Scale bars = 100 μm. (E) Quantification of the percentage of FAPs differentiated into bodipy+ adipocytes under pro-adipogenic conditions 13 d after isolation from uninjured muscles of young or aged mice. (F) Representative Oil-red O staining of muscle cross sections from young and aged mice 14 d post injury (dpi). Scale bars = 400 μm. (G) Quantification of the Oil-red O covered area normalized to the total cross-sectional area of young and aged muscles under uninjured (Un.) conditions or at 7 and 14 dpi. (H) Representative α-smooth muscle actin (α-SMA) immunostaining showing spontaneous fibrogenic differentiation of FAPs 6 d after isolation from uninjured muscles of young or aged mice. Scale bars = 100 μm. (I) Quantification of

the percentage of α-SMA+ FAPs 6 d after isolation from uninjured muscles of young or aged mice. (J) Representative Masson Trichrome staining of cross sections from muscles of young or aged mice under uninjured conditions or at 14 dpi. Fibrotic areas are labeled by the aniline blue component of the staining. Scale bars = 100 μm. (K) Quantification of the aniline blue+ fibrotic area of the Masson Trichrome staining normalized to the total muscle area in cross sections of young and aged muscles under uninjured conditions or at 14 dpi. (L) qPCR quantification of the ratio of intronic (In) to full-length (FL) PDGFRα transcripts in young and aged muscle under uninjured conditions or at 3, 7 and 14 dpi. (M) qPCR quantification of the ratio of In to FL PDGFRα transcripts in FAPs isolated from muscles of young or aged mice at 3 dpi. (B, C, E and I) Cells pooled from up to n=3 mice and n≥15 replicates per condition, repeated three times for each condition. (G, K, L and M) n≥6 mice per condition. (B, C, E, G, I, and K-M) Data are represented as means ± S.E.M. p-values are *p<0.05, **p<0.01, ***p<0.001 using a Mann-Whitney test when comparing two conditions, and an ANOVA followed by a Bonferroni post hoc test when comparing multiple conditions. See also Figures S1 and S2.

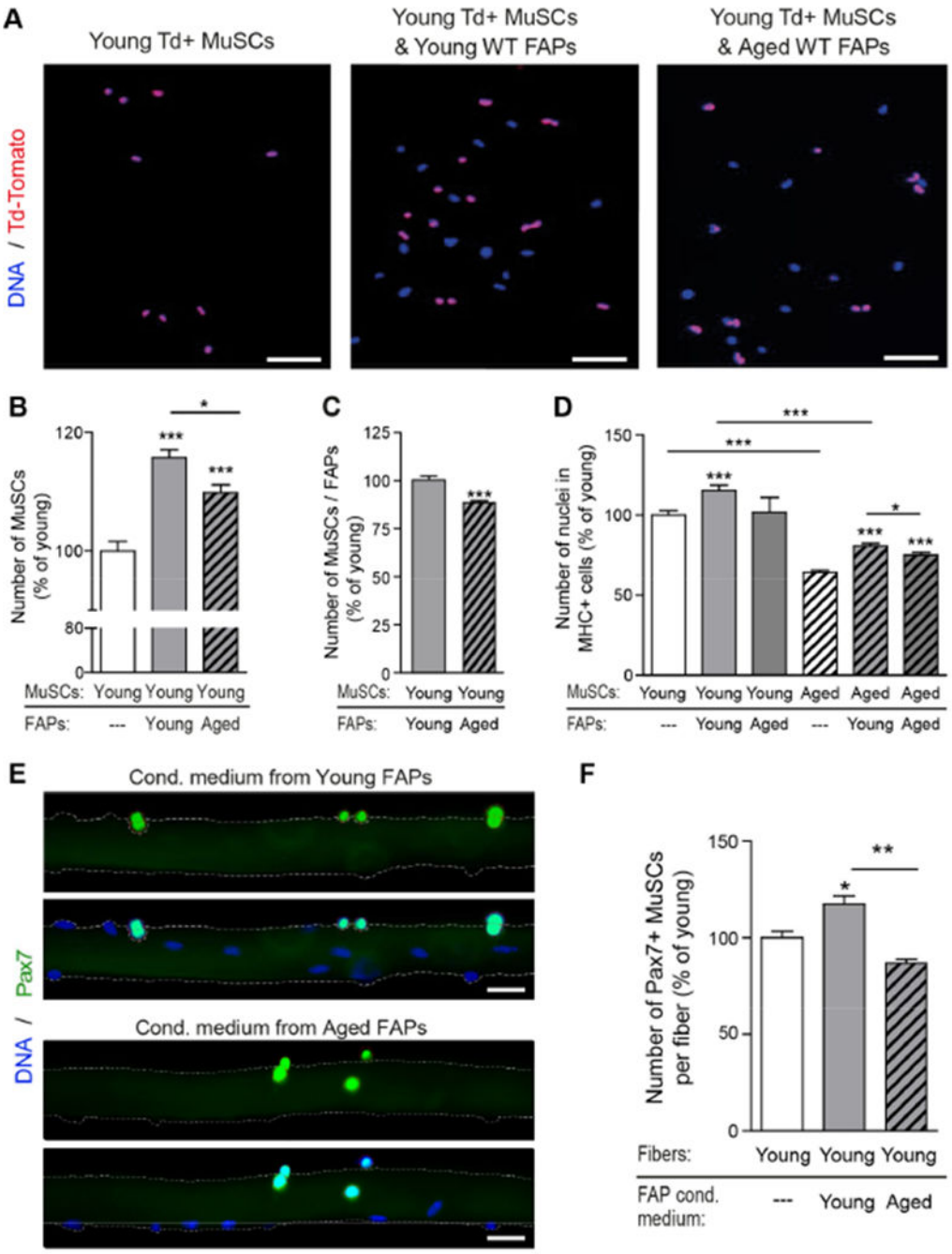

Figure 2. Aged FAPs Fail to Support MuSCs

(A) Representative images of MuSCs from uninjured muscles of young mice with constitutive nuclear Td-Tomato+ (Td+) expression, cultured alone or together with wild-type (WT) FAPs from uninjured young or aged muscles for 12 h after isolation. Scale bars = 50 μm. (B) Quantification of the number of Td+ MuSCs from uninjured muscles of young mice cultured alone or together with WT FAPs from young or aged uninjured muscles for 12 h after isolation. (C) Quantification of the number of Td+ MuSCs from young uninjured muscles relative to WT FAPs from young or aged uninjured muscles co-cultured for 12 h

after isolation. (D) Quantification of the number of nuclei in Myosin Heavy Chain (MHC) positive cells generated by MuSCs from uninjured muscles from young or aged mice, alone or co-cultured with FAPs from young and aged uninjured muscles for 6 d after isolation. Cells pooled from up to n=3 mice and n≥13 replicates per condition, repeated three times for each condition. (E) Representative Pax7 immunostaining of single EDL myofibers that were cultured for 42h after isolation from uninjured muscles of young mice with medium conditioned (Cond.) by FAPs isolated from uninjured muscles of young or aged mice. Scale bars = 25 μm. (F) Quantification of Pax7+ MuSCs on single myofibers that were cultured for 42 h after isolation from uninjured muscles of young mice with control medium or medium conditioned by FAPs isolated from uninjured muscles of young or aged mice. n=3 mice per condition, n≥30 fibers per mouse. (B, C) Cells pooled from up to n=3 mice and n=24 replicates per condition, repeated three times for each condition. (B, C, D and F) Data are represented as means ± S.E.M. p-values are *p<0.05, **p<0.01, ***p<0.001 using a Mann-Whitney test when comparing two conditions, and an ANOVA followed by a Bonferroni post hoc test when comparing multiple conditions. See also Figure S3.

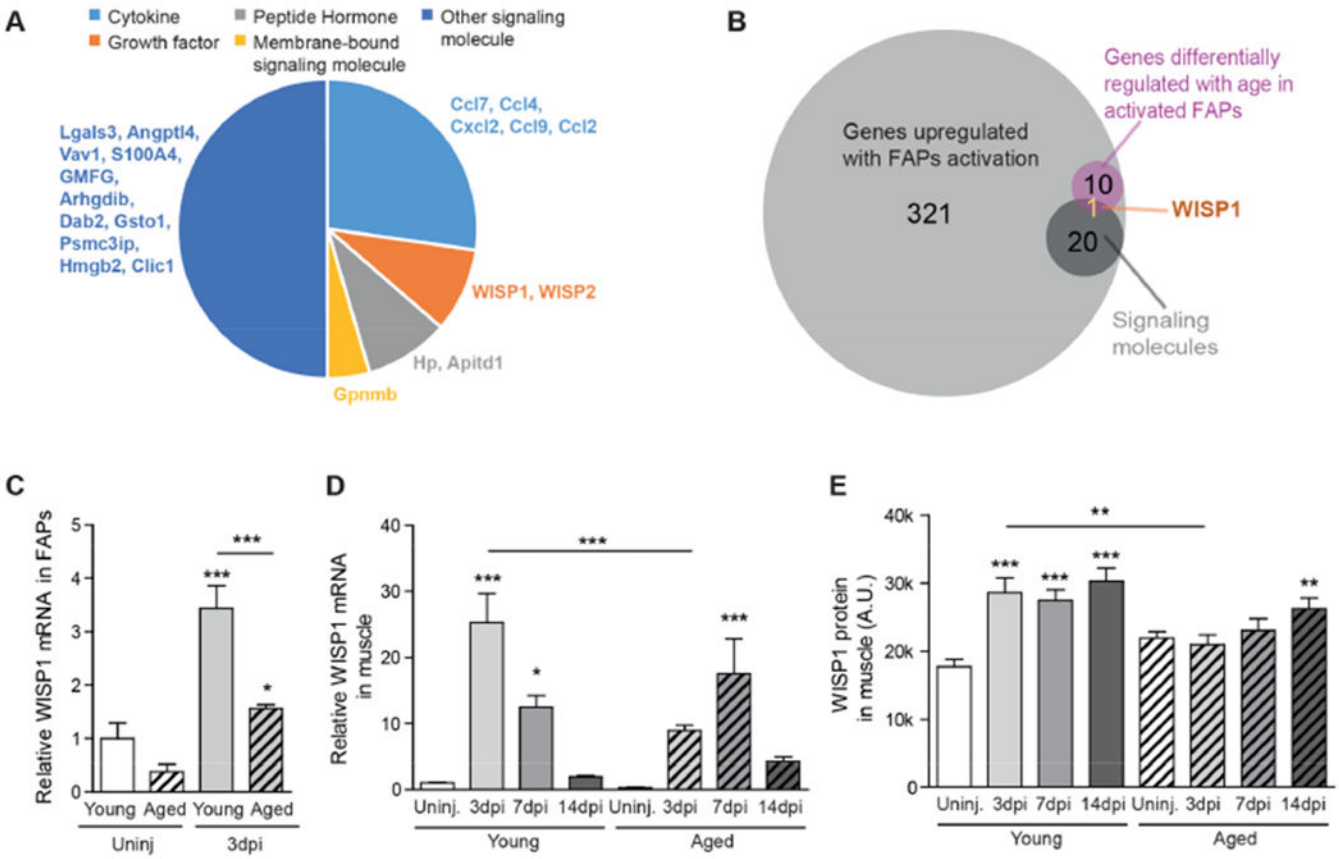

Figure 3. Identification of WISP1 as an Age Affected Matricellular Factor Secreted by FAPs

(A) Pie chart of transcripts detected by genome-wide profiling that are upregulated in FAPs isolated from young muscles at 3 dpi compared to the uninjured condition and classified as secreted proteins. (B) Venn diagram of genes induced in FAPs isolated from young muscles at 3 dpi compared to the uninjured condition (light grey), differentially regulated between FAPs isolated from young and aged muscles at 3 dpi (purple), and encoding proteins annotated as “signaling molecules” by the Panther database (dark grey). (C) WISP1 mRNA levels measured by qPCR in FAPs isolated from young and aged muscles under uninjured conditions or at 3 dpi. (D) WISP1 mRNA levels measured by qPCR in muscles from young and aged mice under uninjured conditions or at 3, 7 and 14 dpi (n=8 mice per condition). (E) WISP1 protein levels in regenerating muscles from young and aged mice under uninjured conditions or at 3, 7 and 14 dpi. n≥5 mice per condition. Arbitrary units (A.U.). (A-C) n≥5 replicates per condition, with cells pooled from multiple mice for each. (C-E) Data are represented as means ± S.E.M. p-values are *p<0.05, **p<0.01, ***p<0.001 using an ANOVA followed by a Bonferroni post hoc test. See also Figures S4 and S5.

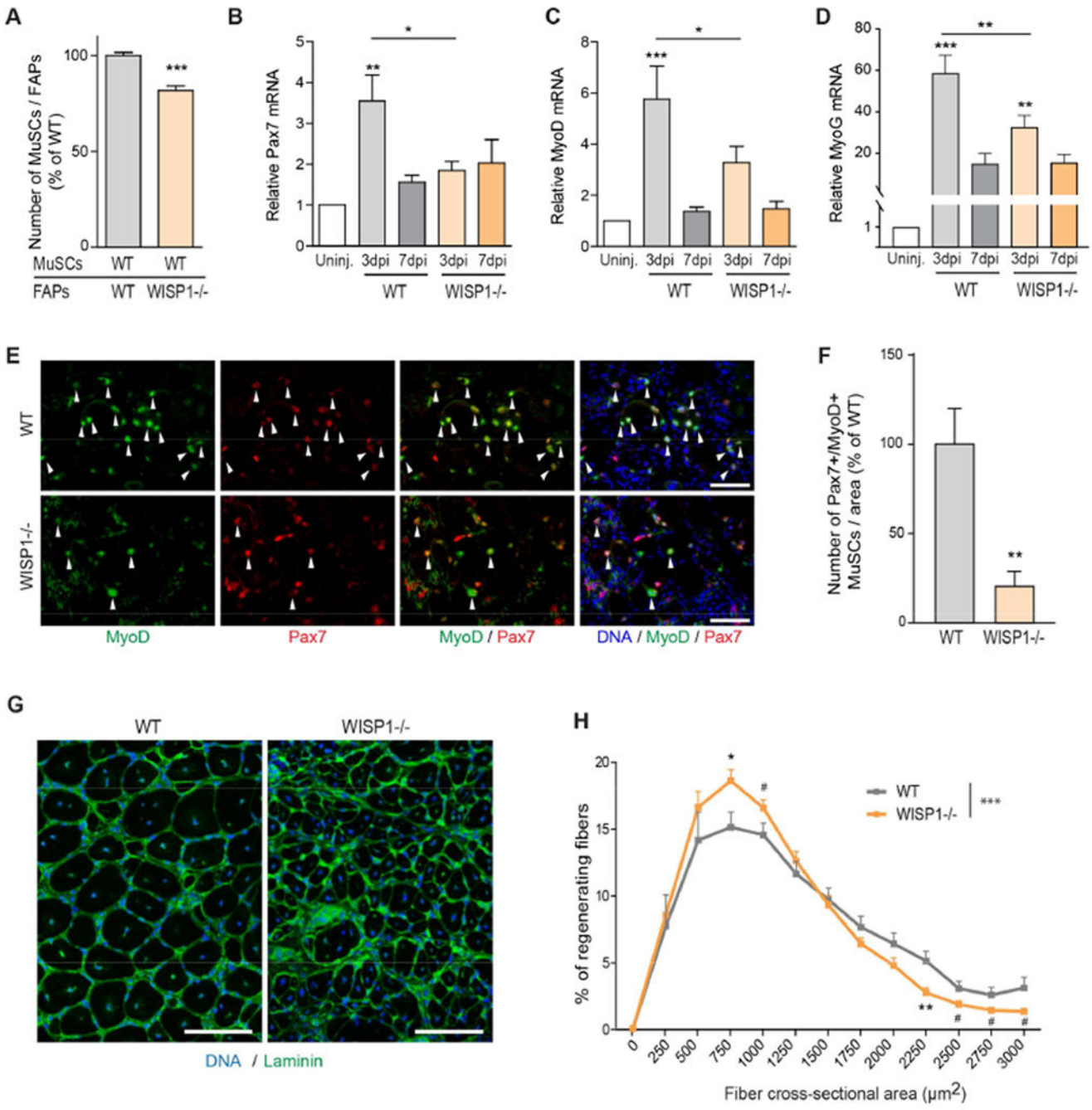

Figure 4. Impaired MuSC Commitment and Muscle Regeneration in WISP1 Knockout Mice

(A) Quantification of the number of Td+ MuSCs from young uninjured muscles relative to co-cultured FAPs from wild-type (WT) or WISP1 knockout (WISP1−/−) muscles for 12 h after isolation. n=24 replicates per condition, repeated twice with cells from different mice for each condition. (B-D) qPCR quantification of Pax7, MyoD and Myogenin (MyoG) mRNA from WT and WISP1−/− muscles under uninjured (uninj.) conditions or at 3 and 7 dpi. (E) Representative Pax7 and MyoD immunostaining of WT and WISP1−/− muscle cross sections at 3 dpi. White arrowheads indicate Pax7+/MyoD+ MuSCs. Scale bar = 100

μm. (F) Quantification of the number of Pax7+/MyoD+ MuSCs in WT and WISP1−/− muscle cross sections at 3 dpi. (G) Representative Laminin immunostaining of WT and WISP1−/− muscle cross sections at 14 dpi. Scale bar = 100 μm. (H) Quantification of the cross-sectional area distribution of regenerating fibers with centralized nuclei in WT and WISP1−/− muscles at 14 dpi. (B-D, F and H) n≥5 mice per condition. (A, B-D, F and H) Data are represented as means ± S.E.M. p-values are *p<0.05, **p<0.01, ***p<0.001, #p<0.1 using a Mann-Whitney test when comparing two conditions, and ANOVA followed by a Bonferroni post hoc test when comparing multiple conditions, and a Kolmogorov-Smirnov test to assess fiber cross-sectional area distributions. See also Figure S6.

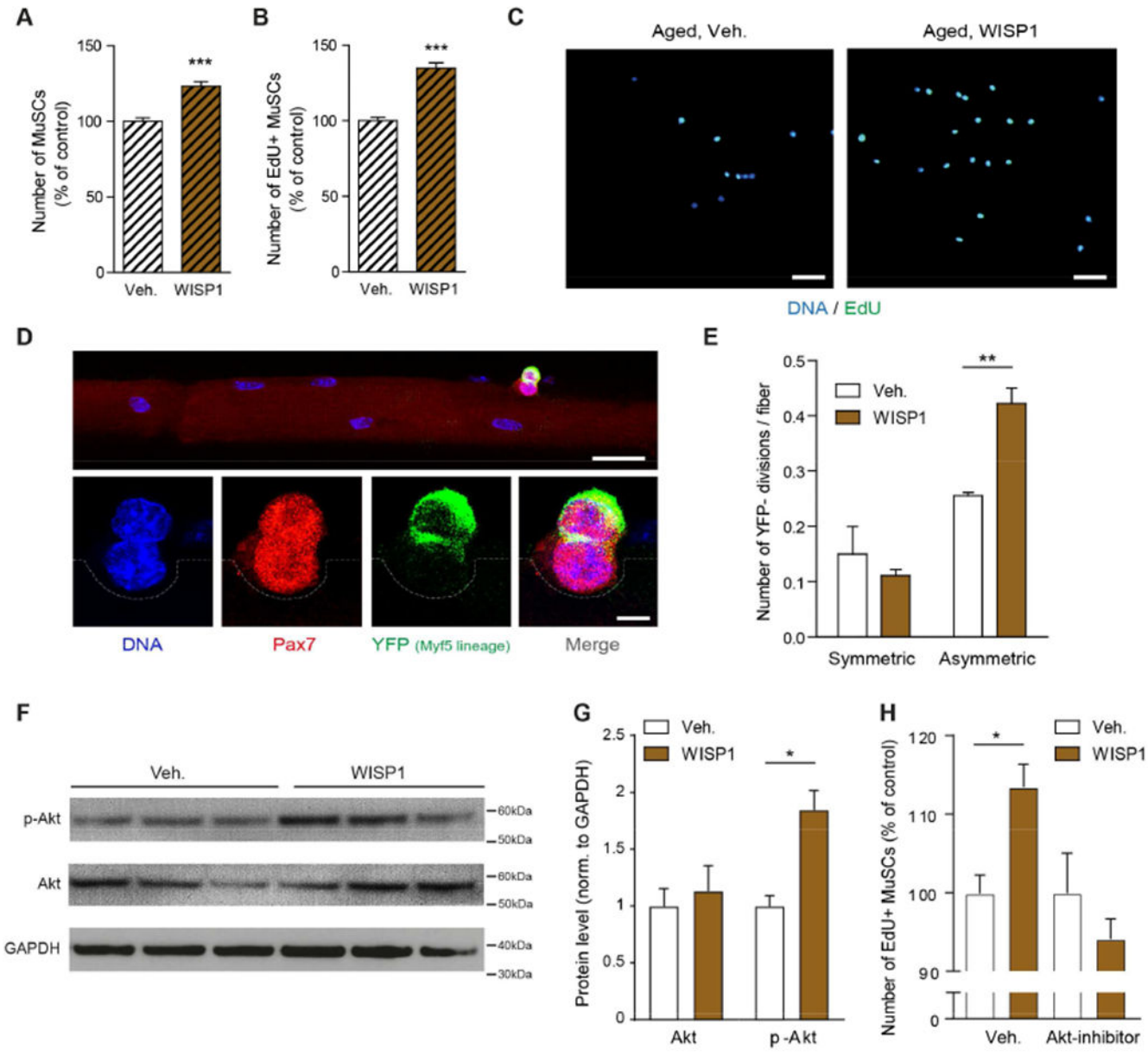

Figure 5. WISP1 Stimulates Asymmetric MuSC Commitment and Activates the Akt Pathway

(A) Quantification of the number of MuSCs cultured for 36 h after isolation from uninjured muscles of aged mice in media containing vehicle (Veh.) or 8 μg/ml WISP1. (B) Quantification of the number of EdU+ MuSCs cultured for 3 days after isolation from uninjured muscles of aged mice in media containing vehicle (Veh.) or WISP1. (C) Representative images of EdU+ MuSCs cultured for 3 days after isolation from uninjured muscles of aged mice in media containing vehicle (Veh.) or WISP1. Scale bars = 50 μm. (D) Pax7 and YFP immunostaining of an asymmetric MuSC division on a single myofiber from a Myf5-Cre/R26R-YFP mouse. Scale bar = 25 μm (top), 5 μm (bottom). (E) Quantification of the number of symmetric (YFP−/YFP−) and asymmetric (YFP−/YFP+) divisions per single myofiber cultured in media containing Veh. or WISP1 for 42 h after isolation from

adult uninjured EDL muscles of Myf5-Cre/R26R-YFP mice. n=3 mice per condition, n≥30 fibers analyzed per mouse. (F and G) Primary myoblasts were treated with either Veh. or WISP1 for 24 h and phospho-Akt (p-Akt) and total Akt protein levels were quantified by western blot and normalized to GAPDH. n=3 replicates per condition. (H) Quantification of the number of EdU+ MuSCs cultured for 3 d after isolation from uninjured muscle of aged mice with media containing Veh. or WISP1 with or without 0.1 μM of the Akt inhibitor MK-2206. (A, B and H) Cells pooled from up to 3 mice and n≥16 replicates per condition, repeated twice for each condition. (A, B, E, G and H) Data are represented as means ± S.E.M. p-values are *p<0.05, **p<0.01, ***p<0.001 using a Mann-Whitney test when comparing two conditions, and an ANOVA followed by a Bonferroni post hoc test when comparing multiple conditions. See also Figure S7.

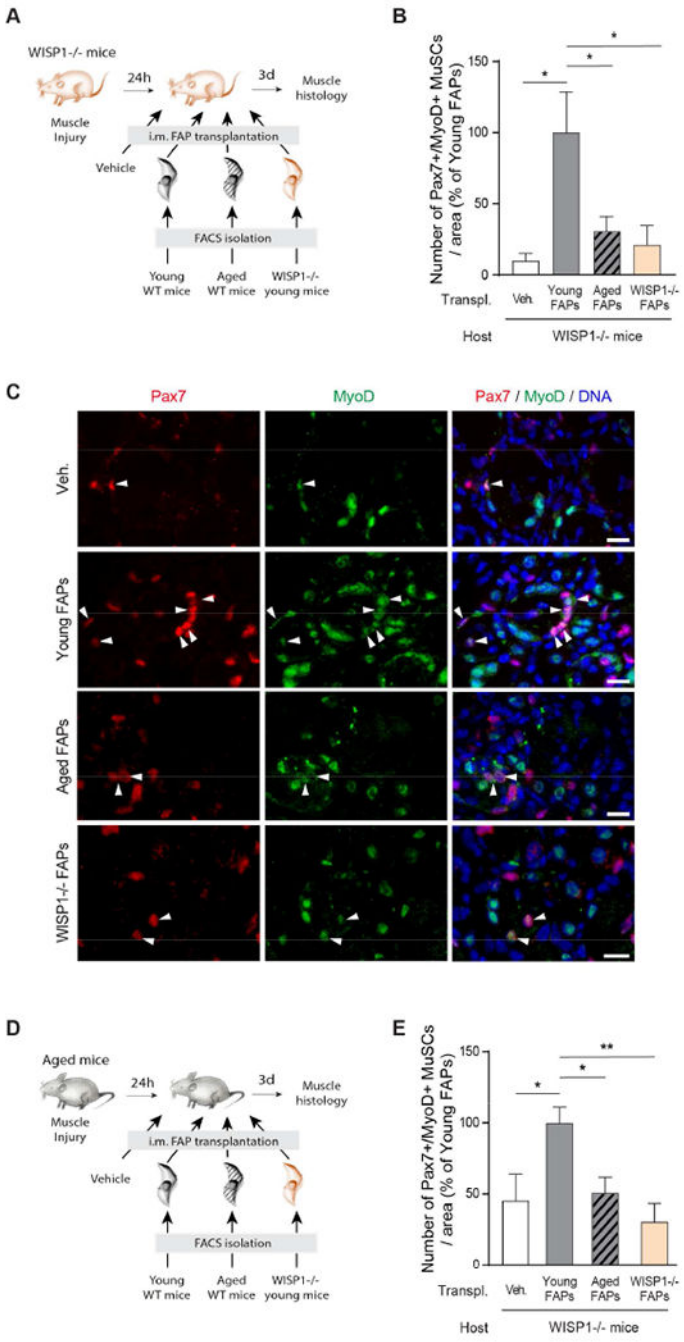

Figure 6. Paracrine WISP1 secretion from young FAPs stimulates the myogenic commitment of aged MuSCs

(A) Experimental overview of the in-vivo transplantation of FAPs in WISP1−/− recipient mice. (B and C) Quantification and representative images of Pax7+/MyoD+ MuSCs by immunofluorescence in muscle cross-sections of WISP1−/− mice at 4dpi, after intra-muscular injection of vehicle or FAPs freshly isolated from young, aged or WISP1−/− mice at 1 dpi. n≥3 mice per condition. (D) Experimental overview of the in-vivo transplantation of FAPs in aged WT recipient mice. (E) Quantification of the number of Pax7+/MyoD+ MuSCs by immunofluorescence in muscle cross-sections of aged WT mice at 4dpi, after

intra-muscular injection of vehicle or FAPs freshly isolated from young, aged or WISP1−/− mice at 1 dpi. n≥4 mice per condition. (B and E) Data are represented as means ± S.E.M. p-values are *<0.05, **p<0.01 using an ANOVA followed by a Bonferroni post hoc test.

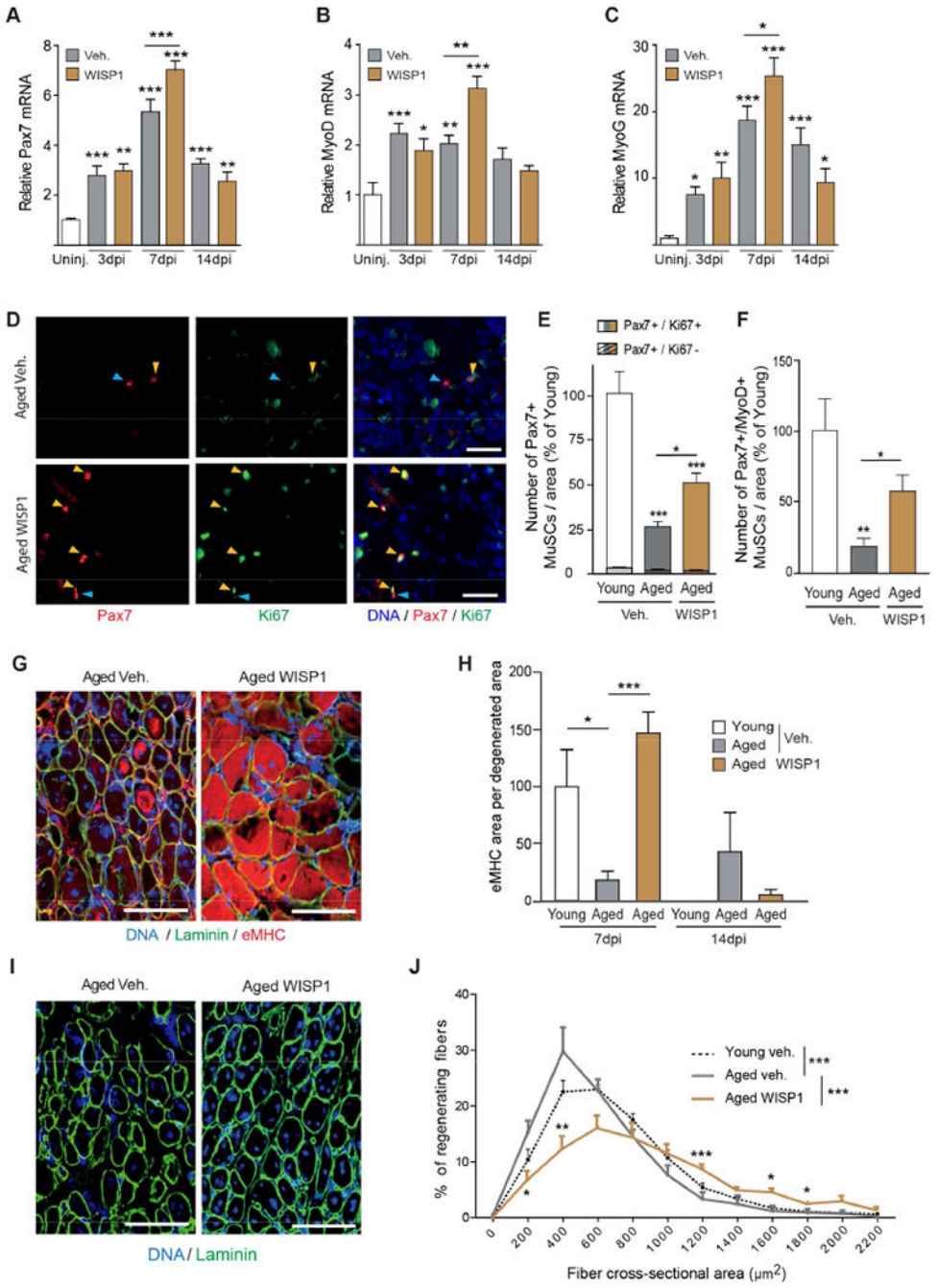

Figure 7. WISP1 Treatment Rejuvenates MuSC Function and Restores Muscle Regeneration

(A-C) qPCR quantification of Pax7, MyoD and MyoG mRNA in muscles of aged mice treated with daily i.p. injection of Veh. or WISP1 at 1mg/kg under uninjured (uninj.) conditions or at 3, 7 and 14 dpi. (D) Representative immunostainings for Pax7 and Ki67 of cross sections of Veh. or WISP1 treated aged muscles at 3 dpi. Yellow and blue arrowheads show Pax7+/Ki67+ and Pax7+/Ki67− MuSCs, respectively. Scale bars = 50 μm. (E) Quantification of the number of Pax7+/Ki67+ and Pax7+/Ki67− MuSCs in cross sections of young and Veh. or WISP1 treated aged muscles at 3 dpi. (F) Quantification of the number of

Pax7+/MyoD+ MuSCs in cross sections of young and Veh. or WISP1 treated aged muscles at 3 dpi. (G) Representative Laminin and embryonic myosin heavy chain (eMHC) immunostainings of cross sections of Veh. or WISP1 treated aged muscles at 7 dpi. Scale bars = 100 μm. (H) Quantification of the area covered by eMHC positive fibers in sections of young and Veh. or WISP1 treated aged muscles at 7 and 14 dpi. (I) Representative Laminin immunostainings of cross sections of Veh. or WISP1 treated aged muscles at 7 dpi. Scale bars = 100 μm. (J) Quantification of the cross-sectional area distribution of regenerating fibers with centralized nuclei in sections of young and aged Veh. or WISP1 treated muscles at 7 dpi. Inter-class statistics are compared to the aged Veh. group. (A-C, E, F, H and J) n≥4 mice per condition. Data are represented as means ± S.E.M. p-values are *<0.05, **p<0.01, ***p<0.001 using an ANOVA followed by a Bonferroni post hoc test when comparing multiple conditions, and a Kolmogorov-Smirnov test to assess fiber cross-sectional area distributions. See also Figure S8.